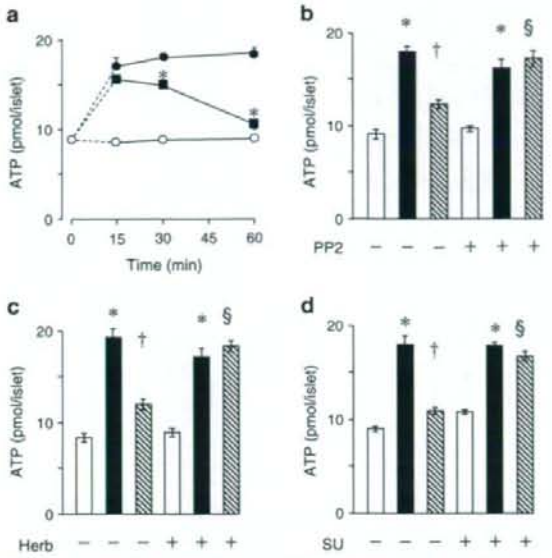

Fig. 1 Effects of Src inhibitors on ATP contents at high glucose after exposure to ouabain. **a** Time-course of ouabain-induced decrease of ATP contents. After preincubation with 2.8 mmol/l glucose, islets were incubated at 2.8 mmol/l glucose (white circles) or 16.7 mmol/l glucose with (black squares) or without (black circles) 1 mmol/l ouabain for the indicated times in Ca^{2+}-depleted condition, and ATP contents were determined. Values are means±SE (n=5). *p<0.01 vs 16.7 mmol/l glucose. **b–d** Effects of Src inhibitors on ouabain-induced decrease of ATP contents in high glucose. After preincubation with 2.8 mmol/l glucose with or without Src inhibitors, islets were incubated for 60 min at 2.8 mmol/l glucose (white bars) or 16.7 mmol/l glucose with (hatched bars) or without (black bars) ouabain in the presence or absence of Src inhibitors under Ca^{2+}-depleted condition, and ATP contents were determined. **b** Effect of 10 μmol/l PP2. **c** Effect of 1 μmol/l herbimycin A (Herb). **d** Effect of 5 μmol/l SU6656 (SU). Values are means±SE of n=8 (**b**), n=10 (**c**) and n=8 (**d**) determinations. *p<0.01 vs 2.8 mmol/l glucose; †p<0.01 vs 16.7 mmol/l glucose; §p<0.01 vs 16.7 mmol/l glucose plus ouabain without Src inhibitors

15 min did not suppress ATP content in the presence of 16.7 mmo/l glucose (at 15 min, 16.7 mmol/l glucose plus ouabain: 15.6±0.2 pmol per islet vs 16.7 mmol/l glucose; p= NS), but such exposure for 30 min decreased ATP content in the presence of 16.7 mmo/l glucose (at 30 min, 16.7 mmol/l glucose plus ouabain: 14.9±0.4 vs 16.7 mmol/l glucose: 18.0±0.4 pmol per islet; p<0.01; Fig. 1a). Furthermore, an exposure for 60 min profoundly suppressed ATP content at high glucose (at 60 min, 16.7 mmol/l glucose plus ouabain: 10.6±0.6 vs 16.7 mmol/l glucose: 18.5±0.6 pmol per islet; p<0.01; Fig. 1a).

In the presence of 10 μmol/l PP2, a Src inhibitor, 1 mmol/l ouabain failed to suppress ATP content in the presence of 16.7 mmol/l glucose (16.7 mmol/l glucose plus ouabain with PP2: 17.2±0.9 vs 16.7 mmol/l glucose with PP2: 16.2±0.9 pmol per islet; p=NS) (Fig. 1b). ATP content in ouabain-treated islets at high glucose in the presence of PP2 was larger than that in the absence of PP2 (16.7 mmol/l glucose plus ouabain with PP2 vs 16.7 mmol/l glucose plus ouabain: 12.3±0.5 pmol per islet; p<0.01). Similar results were observed in experiments using other Src inhibitors (Fig. 1c,d).

Effect of ouabain on ROS production Exposure to 1 mmol/l ouabain for 15 min did not increase CM-DCF fluorescence, which represents ROS production, in the presence of 16.7 mmo/l glucose (at 15 min, 16.7 mmol/l glucose plus ouabain: 1.23±0.11 vs 16.7 mmol/l glucose: 1.08±0.13 relative units; p=NS; Fig. 2a). However, such exposure for 30 or 60 min augmented CM-DCF fluorescence in the presence of 16.7 mmo/l glucose (at 30 min, 16.7 mmol/l glucose plus ouabain: 1.58±0.10 vs 16.7 mmol/l glucose: 1.24±0.07 relative units; p<0.05; at 60 min, 16.7 mmol/l glucose plus ouabain: 1.71±0.12 vs 16.7 mmol/l glucose: 1.29±0.04 relative units; p<0.05; Fig. 2a). In the presence of 10 μmol/l PP2, 1 mmol/l ouabain did not increase CM-DCF fluorescence in the presence of 16.7 mmol/l glucose (16.7 mmol/l glucose plus ouabain with PP2: 1.31±0.07 vs 16.7 mmol/l glucose with PP2: 1.33±0.05 relative units; p= NS) (Fig. 2b). PP2 reduced CM-DCF fluorescence of islet cells in the presence of 16.7 mmol/l glucose and 1 mmol/l ouabain (16.7 mmol/l glucose plus ouabain with PP2 vs 16.7 mmol/l glucose plus ouabain: 1.63±0.08 relative units; p<0.05; Fig. 2b).

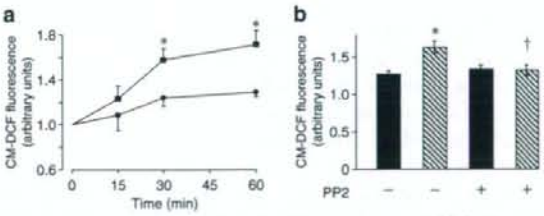

Fig. 2 Effects of Src inhibitor on ROS production at high glucose after exposure to ouabain. **a** Time-course of ouabain-induced increase of ROS production. After fluorescence measurements at time zero, the dispersed islet cells were incubated for the indicated times, with (squares) or without (circles) 1 mmol/l ouabain in the presence of 16.7 mmol/l glucose under Ca^{2+}-depleted conditions. Values are means±SE (n=4) as a ratio of values at time zero. *p<0.05 vs 16.7 mmol/l glucose. **b** Effects of Src inhibitor (PP2) on ouabain-induced increase of ROS production at high glucose. After CM-DCF fluorescence was determined at time zero, islet cells were incubated for 60 min with 16.7 mmol/l glucose with (hatched bars) or without (black bars) 1 mmol/l ouabain in the presence or absence of 10 μmol/l PP2 under Ca^{2+}-depleted conditions, and fluorescence was measured at 60 min. Values are means±SE (n=4) as a ratio of values at time zero. *p<0.05 vs 16.7 mmol/l glucose. †p<0.05 vs 16.7 mmol/l glucose plus ouabain without PP2

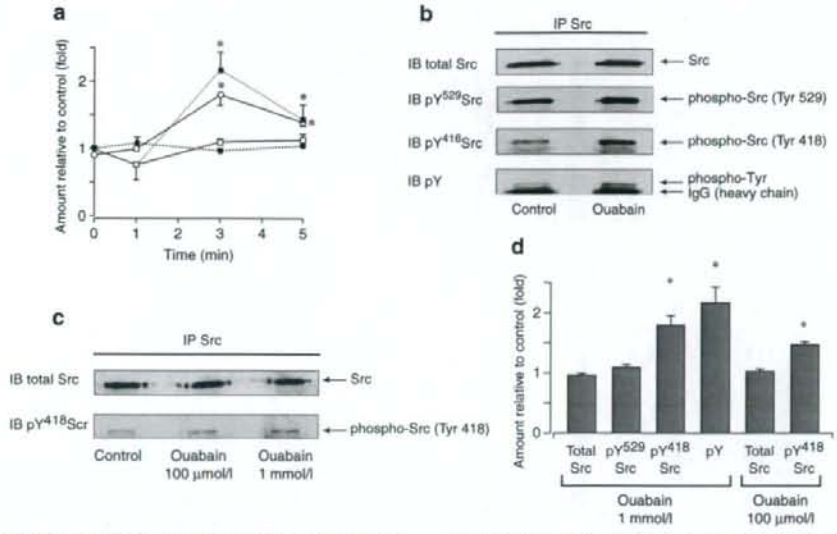

Fig. 3 Ouabain-induced Src tyrosine phosphorylation in islets under Ca^{2+}-deprived condition in the presence of 16.7 mmol/l glucose. **a** Time-course of ouabain-induced Src tyrosine phosphorylation. After preincubation with 2.8 mmol/l glucose, islets were incubated with or without 1 mmol/l ouabain in the presence of 16.7 mmol/l glucose under Ca^{2+}-depleted conditions for the indicated times. Islets were then lysed, immunoprecipitated with an anti-Src antibody, and assayed for Src tyrosine phosphorylation by Western blotting using Tyr^{418} phosphospecific Src antibody (pY^{418}Src, white circles), Tyr^{529} phosphospecific Src antibody (pY^{529}Src, white squares) or phosphotyrosine antibody (pY, black squares) by repetition of stripping and reprobing for the same blot. To ensure equal loading, total Src antibody (total Src, black circles) was also reprobed. Data are expressed relative to control (16.7 mmol/l glucose without ouabain) value (means±SE, 0 min: n=3, 1 min: n=3, 3 min: n=8, 5 min: n=4). *p<0.01 vs control (16.7 mmol/l glucose without ouabain). **b** Representative immunoblots (IB) for total Src antibody, Tyr^{418} or Tyr^{529} phosphospecific Src antibodies (pY^{418}Src and pY^{529}Src) and phosphotyrosine antibody (pY) at 3 min in the same membrane. In the pY immunoblot, blots of IgG heavy chain derived from antibody used during immunoprecipitation were also observed. **c** Dose-dependent effect of ouabain on the level of Src tyrosine phosphorylation in islets. Representative immunoblot (IB) for total Src antibody and pY^{418}Src antibody at 3 min in the same membrane. **d** Quantification data are expressed as means±SE of n=6 (100 µmol/l ouabain), n=8 (1 mmol/l ouabain) determinations relative to control (16.7 mmol/l glucose without ouabain) values. *p<0.01 vs control (16.7 mmol/l glucose without ouabain). IP, immunoprecipitated

Effect of ouabain on Src phosphorylation Src activity is regulated by the phosphorylation of Tyr^{418} and Tyr^{529}. Either a decrease in phosphorylation of Tyr^{529} or an increase in phosphorylation of Tyr^{418} stimulates Src kinase activity. Ouabain (1 mmol/l) caused a rapid activation of Src in the presence of 16.7 mmol/l glucose under Ca^{2+}-deprived conditions. The maximum increase in Tyr^{418} phospholyration was observed 3 min after ouabain exposure (Fig. 3a). Ouabain caused a significant increase in Try^{418} and total tyrosine phosphorylation, but had no effect on Try^{529} phosphorylation (at 3 min, fold increase relative to control, pY^{418}Src: 1.79±0.15, p<0.01 vs control; total tyrosine phosphorylation (pY): 2.17±0.26, p<0.01 vs control; pY^{529}Src: 1.09±0.04, p=NS vs control; total Src: 0.96±0.03, p=NS vs control) (Fig. 3b,d). A dose-dependent effect of ouabain on Tyr^{418} phosphorylation was also observed (100 µmol/l ouabain, at 3 min, fold increase relative to control, pY^{418}Src: 1.47±0.05, p<0.01 vs control; total Src: 1.02±0.04, p=NS vs control; Fig. 3c,d). Such effects of ouabain on Src phosphorylation were also observed in a medium containing a physiological concentration of Ca^{2+}(fold increase relative to control, pY^{418}Src: 1.59±0.10, p<0.01 vs control; pY^{529}Src: 1.07±0.07, p=NS vs control; total Src: 0.96±0.06, p=NS vs control) (Fig. 4).

Effect of ouabain on $\Delta\Psi_m$ To evaluate the effect of ouabain on $\Delta\Psi_m$, JC-1 fluorescence was measured in the presence of 16.7 mmol/l glucose without Ca^{2+} (Fig. 5). After addition of 16.7 mmol/l glucose to the medium, fluorescence increased gradually, indicating hyperpolarisation of mitochondrial membrane potential, whereas the basal level of fluorescence was unchanged in the presence of 2.8 mmol/l glucose. Ouabain (1 mmol/l) significantly inhibited glucose-induced hyperpolarisation of mitochondrial membrane potential 30 min after administration (at 30 min, 16.7 mmol/l glucose plus ouabain: 1.04±0.03 vs 16.7 mmol/l glucose: 1.51±0.05 relative units; p<0.01). However, in the presence of 1 mmol/l ouabain with 16.7 mmol/l glucose, 10 µmol/l PP2 reversed the effect of ouabain on $\Delta\Psi_m$ and increased JC-1 fluorescence 30 min

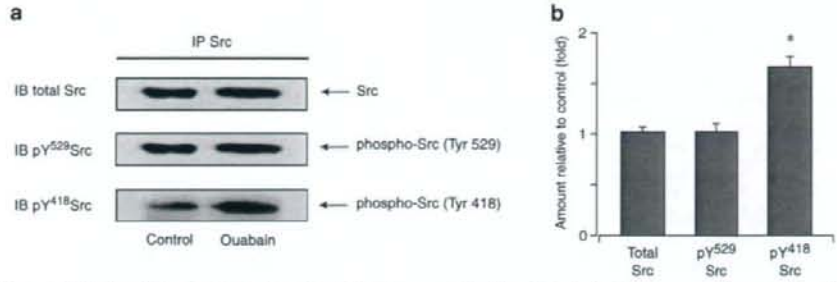

Fig. 4 Ouabain (1 mmol/l)-induced Src tyrosine phosphorylation in islets in medium containing a physiological concentration of Ca^{2+} (2.8 mmol/l) in the presence of 16.7 mmol/l glucose. **a** Representative immunoblot (IB) for total Src antibody and pY^{418}Src or pY^{529}Src antibodies at 3 min in the same membrane. **b** Quantification data from $n=5$ independent experiments. Data are expressed relative to control values (means±SE). *$p<0.01$ vs control (16.7 mmol/l glucose without ouabain). IP, immunoprecipitated

after administration (16.7 mmol/l glucose plus ouabain with PP2: 1.41±0.07 vs 16.7 mmol/l glucose plus ouabain: 1.04±0.03 relative units; $p<0.01$). JC-1 fluorescence decreased to below the basal level after the addition of 1 μmol/l FCCP.

Effect of ouabain on glucose oxidation Glucose oxidation in islets in the presence of 16.7 mmol/l glucose was increased compared with that in the presence of 2.8 mmol/l glucose (Fig. 6). Glucose oxidation with 2.8 mmol/l glucose was not affected by 1 mmol/l ouabain (ouabain plus 2.8 mmol/l glucose: 7.6±1.0 vs 2.8 mmol/l glucose: 5.6± 0.6 pmol $islet^{-1}$ 90 min^{-1}; p=NS). However, glucose oxidation with 16.7 mmol/l glucose was suppressed by the agent (16.7 mmol/l glucose plus ouabain: 30.0±4.3 vs 16.7 mmol/l glucose: 53.9±6.1 pmol $islet^{-1}$ 90 min^{-1}; $p<0.01$). In the presence of PP2 or α-tocopherol plus ascorbate, ouabain did not affect glucose oxidation at 16.7 mmol/l glucose. Glucose oxidation with 16.7 mmol/l glucose and ouabain in the presence of PP2 or α-tocopherol plus ascorbate was larger than that in the absence of PP2 and α-tocopherol plus ascorbate (16.7 mmol/l glucose plus ouabain with PP2: 50.2±4.5 vs 16.7 mmol/l glucose plus ouabain: 30.0±4.3; $p<0.01$; 16.7 mmol/l glucose plus ouabain with α-tocopherol plus ascorbate: 45.6± 3.2 pmol $islet^{-1}$ 90 min^{-1} vs 16.7 mmol/l glucose plus ouabain; $p<0.01$).

Characteristics of animals and islets Table 1 shows the characteristics of the diabetes model GK rats and control Wistar rats used in this study. GK rats had lower body weight than control Wistar rats. In the fed state, GK rats had higher plasma glucose concentration. DNA content and

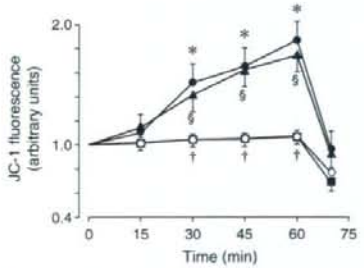

Fig. 5 Time-course effects of Src inhibitor (PP2) on ouabain-induced decrease of mitochondrial membrane potential at high glucose. After JC-1 was loaded, dispersed islet cells were preincubated for 30 min at 2.8 mmol/l glucose with or without 10 μmol/l PP2. At time zero, basal fluorescence was determined, and islet cells were incubated for the indicated time periods in Ca^{2+} -depleted conditions at 2.8 mmol/l glucose (white circles) or 16.7 mmol/l glucose with (black squares) or without (black circles) 1 mmol/l ouabain, or with 16.7 mmol/l glucose with 1 mmol/l ouabain in the presence of 10 μmol/l PP2 (black triangles). At 60 min, 1 μmol/l FCCP was added to the medium. Values are means±SE ($n=6$) as a ratio of values at time zero. *$p<0.01$, 2.8 mmol/l vs 16.7 mmol/l glucose; †$p<0.01$, 16.7 mmol/l glucose vs 16.7 mmol/l glucose + ouabain; §$p<0.01$, 16.7 mmol/l glucose + ouabain vs 16.7 mmol/l glucose + ouabain + PP2

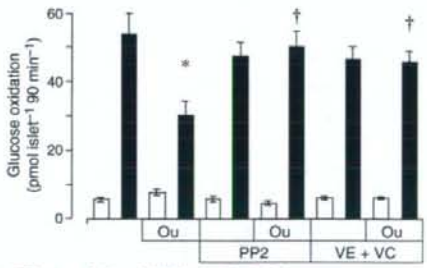

Fig. 6 Effects of Src inhibitor and ROS scavenger on ouabain-induced decrease of glucose oxidation at high glucose. After preincubation with 2.8 mmol/l glucose with or without Src inhibitor and ROS scavenger, islets were incubated for 90 min at 2.8 mmol/l glucose (white bars) or 16.7 mmol/l glucose (black bars) with or without 1 mmol/l ouabain (Ou) in the presence or absence of Src inhibitor (10 μmol/l PP2) and ROS scavenger (100 μmol/l α-tocopherol plus 200 μmol/l ascorbate, VE+VC) under Ca^{2+}-depleted conditions, and glucose oxidation was determined. Values are means ±SE of $n=11$ determinations. *$p<0.01$ vs 16.7 mmol/l glucose; †$p<0.01$ vs 16.7 mmol/l glucose plus ouabain without PP2 and α-tocopherol plus ascorbate

Table 1 Characteristics of control Wistar and diabetic GK rats used in the experiments

Characteristics	Control Wistar	GK
Bodyweight (g)	204±1 (45)	163±1** (78)
Non-fasting plasma glucose (mmol/l)	5.83±0.11 (45)	8.83±0.11** (78)
Islet DNA content (ng/islet)	13.5±0.6 (80)	13.5±0.7 (80)
Islet insulin content (ng/islet)	21.8±0.9 (80)	24.2±1.0 (80)

Data are means±SE for the number of observations shown in parentheses

**$p<0.01$ vs control Wistar rat

insulin content of islets derived from GK rats did not differ from those derived from control Wistar rats.

Effect of Src inhibition and ROS scavenger on insulin release and ATP content of GK islets In the presence of 16.7 mmol/l glucose, insulin release from GK islets was reduced compared with control Wistar rats (GK: 1.78± 0.25 vs Wistar: 4.36±0.23 ng islet^{-1} 30 min^{-1}; $p<0.01$) (Fig. 7a). PP2 and α-tocopherol plus ascorbate had no effect on high glucose-induced insulin release from Wistar islets (Fig. 7a,b). However, high glucose-induced insulin release from GK islets was restored to control levels by Src inhibitor (16.7 mmol/l glucose with PP2: 5.05±0.43 vs 16.7 mmol/l glucose: 1.78±0.25 ng islet^{-1} 30 min^{-1}; $p<0.01$) and ROS scavenger (16.7 mmol/l glucose with α-tocopherol plus ascorbate: 4.22±0.60 vs 16.7 mmol/l glucose: 2.13±0.42 ng islet^{-1} 30 min^{-1}; $p<0.01$; Fig. 7a,b). The ATP content of GK islets in the presence of 2.8 mmol/l glucose was not different from that in the presence of 16.7 mmol/l glucose (2.8 mmol/l glucose: 7.0±0.4 vs 16.7 mmol/l glucose: 8.3±0.7 pmol/islet; p=NS; Fig. 7c). In GK islets, ouabain did not suppress ATP content (16.7 mmol/l glucose plus ouabain: 7.7±0.6 pmol/islet vs 16.7 mmol/l glucose; p=NS), while PP2 and α-tocopherol plus ascorbate increased ATP content in the presence of 16.7 mmol/l glucose (16.7 mmol/l glucose with PP2: 12.3± 0.7 pmol/islet vs 16.7 mmol/l glucose, $p<0.01$; 16.7 mmol/l glucose with α-tocopherol plus ascorbate: 11.0±0.7 pmol/islet vs 16.7 mmol/l glucose, $p=0.01$; Fig. 7c).

Effect of Src inhibition and ROS scavenger on ROS production by GK islet cells Ouabain had no effect on ROS production in the presence of high glucose in GK islet cells (at 60 min, 16.7 mmol/l glucose plus ouabain: 2.19±0.18 vs 16.7 mmol/l glucose: 2.42±0.27 relative units; p=NS; Fig. 8a). However, PP2 and α-tocopherol plus ascorbate decreased ROS production in the presence of high glucose in GK islet cells (at 60 min, 16.7 mmol/l glucose with PP2: 1.53±0.08 relative units vs 16.7 mmol/l glucose, $p<0.05$; 16.7 mmol/l glucose with α-tocopherol plus ascorbate: 1.46±0.04 relative units vs 16.7 mmol/l glucose, $p<0.05$; Fig. 8b).

Discussion

In the present study, we show that Src plays a role in the signal-transducing function of Na^+/K^+-ATPase, by which ROS generation decreases ATP production in control islets. Moreover, ROS generated by Src activation plays an important role in impaired glucose-induced insulin secretion in GK islets, in which Src activation is ouabain independent.

In pancreatic beta cells, ROS production via non-mitochondrial and mitochondrial pathways has been proposed. ROS production from non-mitochondrial pathways including the hexosamine pathway [23], an unknown pathway from D-glyceraldehyde [24], and NADPH oxidase [25] have been reported. However, in most tissues, the major biological process leading to generation of ROS is the electron transport chain associated with the mitochondrial membrane [26, 27]. Recent studies have shown that beta cells exposed to high glucose produce mitochondrial ROS [14, 15]. Increase in ROS in the presence of high

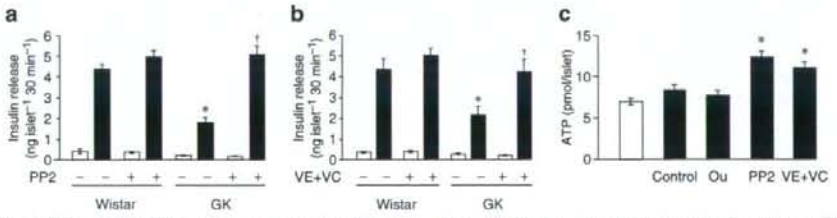

Fig. 7 Effects of Src inhibitor and ROS scavenger on insulin release and ATP contents in GK islets. After preincubation with 2.8 mmol/l glucose for 30 min, islets were incubated at 2.8 mmol/l glucose (white bars) or 16.7 mmol/l glucose (black bars) with or without test materials for 30 min (**a**, **b**) or 60 min (**c**). PP2 and α-tocopherol plus ascorbate were also included during preincubation. **a** Effects of 10 μmol/l PP2 on insulin release from control Wistar islets and GK islets. Values are means±SE (n=10). *$p<0.01$ vs Wistar, 16.7 mmol/l glucose; †$p<0.01$ vs GK, 16.7 mmol/l glucose without PP2. **b** Effects of 100 μmol/l α-tocopherol plus 200 μmol/l ascorbate (VE+VC) on ATP contents in GK islets. After incubation as indicated for 60 min in Ca^{2+}-depleted conditions, ATP contents were determined. Values are means±SE (n=10). *$p<0.01$ vs 16.7 mmol/l glucose

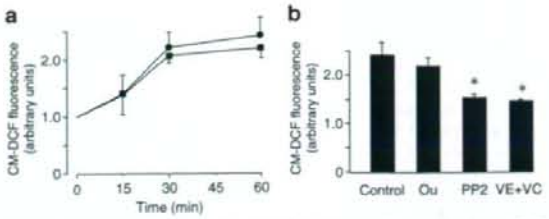

Fig. 8 Effects of ouabain, Src inhibitor and ROS scavenger on ROS production at high glucose in GK islet cells. **a** Effect of 1 mmol/l ouabain on the time-course of high glucose-induced increase of ROS production. After fluorescence measurements at time zero, the dispersed islet cells were incubated for the indicated times with (squares) or without (circles) 1 mmol/l ouabain in the presence of 16.7 mmol/l glucose under Ca^{2+}-depleted conditions. Values are means±SE (n=3) as a ratio of values at time zero. **b** Effects of 1 mmol/l ouabain (Ou), 10 μmol/l PP2 and 100 μmol/l α-tocopherol plus 200 μmol/l ascorbate (VE + VC) on ROS production in the presence of 16.7 mmol/l glucose in GK islet cells. After CM-DCF fluorescence was determined at time zero, islet cells were incubated for 60 min with 16.7 mmol/l glucose in the presence or absence of test materials under Ca^{2+}-depleted conditions, and fluorescence was measured at 60 min. Values are means±SE (n=3) as a ratio of values at time zero. *$p<0.05$ vs 16.7 mmol/l glucose

glucose may be attributable to $\Delta\Psi_m$-dependence of ROS formation, in which an exponential increase in ROS production is observed above 140 mV in mitochondrial membrane potential [28]. However, in the present study, we show for the first time that there is an increase in mitochondrial ROS production via intracellular signal transduction in pancreatic islets. Thus, ROS production via the signal-transducing function of Na^+/K^+-ATPase does not necessarily require hyperpolarisation of mitochondrial membrane potential, as ouabain increases ROS production while the agent simultaneously inhibits hyperpolarisation of mitochondrial membrane potential.

Src is a 60 kDa membrane-associated non-receptor tyrosine kinase that regulates various signal transduction pathways. Src production is widespread and has been demonstrated in pancreatic islets and in a beta cell line [29–32]. Its catalytic activity is controlled by tyrosine phosphorylation and protein–protein interaction. Phosphorylation of Tyr^{529} on Src holds the kinase in an inactive conformation through an intramolecular interaction with its Src homology 2 domain, whereas phosphorylation of Tyr^{418} activates Src by disrupting the intramolecular interaction and creating the substrate-binding site [33]. The binding of ouabain to the Na^+/K^+-ATPase causes rapid activation of Src in various cells including cardiac myocytes [34], smooth muscle cells [34, 35] and kidney epithelial cells [36] independently of the changes in intracellular ion concentrations. In the present study, ouabain stimulated Tyr^{418} phosphorylation but had no effect on Tyr^{529} phosphorylation, a phenomenon also observed in different types of cells [36]. Since ouabain-induced direct interaction between the Na^+/K^+-ATPase α_1 subunit and Src is observed in kidney epithelial cells [36], ouabain-induced direct interaction between Na^+/K^+-ATPase and Src may well be involved in ouabain-induced Src phosphorylation in pancreatic beta cells.

A signal-transducing function of Na^+/K^+-ATPase via Src activation has been proposed recently in different types of cells including cardiac myocytes, A7r5 cells and HeLa cells [37]. The binding of ouabain to Na^+/K^+-ATPase activates Src, resulting in transactivation of the EGF receptor and increased mitochondrial production of ROS independently of changes in intracellular ion concentrations. In the present study, PP2, a specific Src inhibitor that reduces Src kinase activity and Tyr^{418} phosphorylation in rat islets [32], was found to decrease ouabain-induced ROS production, indicating that this signal-transducing function of Na^+/K^+-ATPase plays a role in regulating mitochondrial ROS production in islets. However, the involvement of the transactivation of the EGF receptor in this pathway in islets remains unknown.

In a previous study, we found that ouabain reduces not only the increment in ATP content and the hyperpolarisation of mitochondrial membrane potential by glucose, but also the increment in O_2 consumption by glucose [17]. Since increased O_2 consumption occurs in uncoupling [38], ouabain-induced suppression of mitochondrial ATP production clearly is not mediated by uncoupling, and the suppression may derive from direct or indirect effects on the respiratory chain. Ouabain (1 mmol/l) was found to reduce glucose oxidation in the presence of 16.7 mmol/l glucose in islets in medium containing a physiological level of Ca^{2+} [39]. In the present study, 1 mmol/l ouabain also suppressed glucose oxidation in the presence of 16.7 mmol/l glucose in Ca^{2+}-depleted conditions. Since ouabain-induced suppression of glucose oxidation was restored by ROS scavenger and by Src inhibitor, increased ROS production derived from Src activation may well suppress mitochondrial metabolism in the Krebs cycle, in which CO_2 is released in the reaction mediated by dehydrogenases. This is supported by the fact that administration of 50 μmol/l H_2O_2, a concentration nearly equivalent to the 1 mmol/l ouabain-induced increase in ROS production [17], to mitochondria reduced activity of Krebs cycle enzymes including aconitase, α-ketoglutarate dehydrogenase and succinate dehydrogenase, whose activities declined 96%, 39% and 37%, respectively [40]. Considered together, these findings suggest that ouabain-induced mitochondrial ROS suppresses mitochondrial metabolism in the Krebs cycle, subsequently reducing NADH supply to the respiratory chain, hyperpolarisation of mitochondrial membrane potential, O_2 consumption and ATP production.

We then investigated the role of ROS generated by Src activation in impaired glucose-induced insulin secretion in

diabetes. One of the characteristics of type 2 diabetes is that the insulin secretory response of beta cells to glucose is selectively impaired [41]. In the GK rat, a genetic model of type 2 diabetes mellitus [42], glucose-induced insulin secretion is selectively impaired [43]. On single-channel recording, the glucose sensitivity of the beta cell K_{ATP} channel is remarkably reduced in GK rats, while the inhibitory effect of ATP on channel activity is not significantly different in control and GK rats [5]. The intracellular ATP elevation induced by high glucose is impaired in GK rats [44] as well as in patients with type 2 diabetes [45]. Thus, the impaired insulinotrophic action of glucose in beta cells of GK rats may be attributable to insufficient closure of the K_{ATP} channel because of deficient ATP production derived from impaired glucose metabolism. While there is evidence that islets in GK rats (a diabetes model) and human type 2 diabetes are oxidatively stressed [46, 47], the association between oxidative stress and impaired intracellular ATP elevation in islets is unclear. In the present study, both Src inhibitor and ROS scavenger restored the impairment in high glucose-induced insulin release and ATP elevation in GK islets but had no such effects in control islets. Moreover, Src inhibitor reduced the high glucose-induced increase in ROS generation in GK islet cells but had no effect on that in control islet cells. Ouabain had no effect on ATP content and ROS production in the presence of high glucose despite the prominent recovery effect of Src inhibitor in GK islets, suggesting that Src is endogenously activated independently of ouabain. Taken together, these results indicate that ROS generated by Src activation plays an important role in impaired glucose-induced insulin secretion derived from impaired glucose metabolism in GK islets.

Acknowledgements The authors thank T. Yamaguchi for technical assistance. This study was supported by Scientific Research Grants, a Grant for Leading Project for Biosimulation from the Ministry of Education, Culture, Sports, Science and Technology of Japan, and a grant from Core Research for Evolutional Science and Technology (CREST) of Japan Science and Technology Cooperation.

Duality of interest The authors declare that there is no duality of interest associated with this manuscript.

References

1. Maechler P, Wollheim CB (2001) Mitochondrial function in normal and diabetic β-cells. Nature 414:807–812
2. Kennedy ED, Maechler P, Wollheim CB (1998) Effects of depletion of mitochondrial DNA in metabolism secretion coupling in INS-1 cells. Diabetes 47:374–380
3. Tsuruzoe K, Araki E, Furukawa N et al (1998) Creation and characterization of a mitochondrial DNA-depleted pancreatic β-cell line: impaired insulin secretion induced by glucose, leucine, and sulfonylureas. Diabetes 47:621–631
4. Takehiro M, Fujimoto S, Shimodahira M et al (2005) Chronic exposure to β-hydroxybutyrate inhibits glucose-induced insulin release from pancreatic islets by decreasing NADH contents. Am J Physiol 288:E372–E380
5. Tsuura Y, Ishida H, Okamoto Y et al (1993) Glucose sensitivity of ATP-sensitive K^+ channels is impaired in β-cells of the GK rat. A new genetic model of NIDDM. Diabetes 42:1446–1453
6. Hughes SJ, Faehling M, Thorneley CW, Proks P, Ashcroft FM, Smith PA (1998) Electrophysiological and metabolic characterization of single β-cells and islets from diabetic GK rats. Diabetes 47:73–81
7. Anello M, Lupi R, Spampinato D et al (2005) Functional and morphological alterations of mitochondria in pancreatic beta cells from type 2 diabetic patients. Diabetologia 48:282–289
8. Nabe K, Fujimoto S, Shimodahira M et al (2006) Diphenylhydantoin suppresses glucose-induced insulin release by decreasing cytoplasmic H^+ concentration in pancreatic islets. Endocrinology 147:2717–2727
9. Radu RG, Fujimoto S, Mukai E et al (2005) Tacrolimus suppresses glucose-induced insulin release from pancreatic islets by reducing glucokinase activity. Am J Physiol 288: E365–E371
10. Patane G, Anello M, Piro S, Vigneri R, Purrello F, Rabuazzo AM (2002) Role of ATP production and uncoupling protein-2 in the insulin secretory defect induced by chronic exposure to high glucose or free fatty acids and effects of peroxisome proliferator-activated receptor-γ inhibition. Diabetes 51:2749–2756
11. Joseph JW, Koshkin V, Saleh MC et al (2004) Free fatty acid-induced β-cell defects are dependent on uncoupling protein 2 expression. J Biol Chem 279:51049–51056
12. Maechler P, Jornot L, Wollheim CB (1999) Hydrogen peroxide alters mitochondrial activation and insulin secretion in pancreatic beta cells. J Biol Chem 274:27905–27913
13. Krippeit-Drews P, Kramer C, Welker S, Lang F, Ammon HP, Drews G (1999) Interference of H_2O_2 with stimulus-secretion coupling in mouse pancreatic β-cells. J Physiol 514:471–481
14. Bindokas VP, Kuznetsov A, Sreenan S, Polonsky KS, Roe MW, Philipson LH (2003) Visualizing superoxide production in normal and diabetic rat islets of Langerhans. J Biol Chem 278:9796–9801
15. Sakai K, Matsumoto K, Nishikawa T et al (2003) Mitochondrial reactive oxygen species reduce insulin secretion by pancreatic β-cells. Biochem Biophys Res Commun 300:216–222
16. Lambert AE, Henquin JC, Malvaux P (1974) Cationic environment and dynamics of insulin secretion. IV. Effect of ouabain. Horm Metab Res 6:470–475
17. Kajikawa M, Fujimoto S, Tsuura Y et al (2002) Ouabain suppresses glucose-induced mitochondrial ATP production and insulin release by generating reactive oxygen species in pancreatic islets. Diabetes 51:2522–2529
18. Kometiani P, Li J, Gnudi L, Kahn BB, Askari A, Xie Z (1998) Multiple signal transduction pathways link Na^+/K^+-ATPase to growth-related genes in cardiac myocytes. J Biol Chem 273:15249–15256
19. Xie Z, Kometiani P, Liu J, Li J, Shapiro JI, Askari A (1999) Intracellular reactive oxygen species mediate the linkage of Na^+/K^+-ATPase to hypertrophy and its marker genes in cardiac myocytes. J Biol Chem 274:19323–19328
20. Liu J, Tian J, Haas M, Shapiro JI, Askari A, Xie Z (2000) Ouabain interaction with cardiac Na^+/K^+-ATPase initiates signal cascades independent of changes in intracellular Na^+ and Ca^{2+} concentrations. J Biol Chem 275:27838–27844
21. Fujimoto S, Ishida H, Kato S et al (1998) The novel insulinotropic mechanism of pimobendan: direct enhancement of the exocytotic process of insulin secretory granules by increased Ca^{2+} sensitivity in β-cells. Endocrinology 139:1133–1140

22. Fujimoto S, Tsuura Y, Ishida H et al (2000) Augmentation of basal insulin release from rat islets by preexposure to a high concentration of glucose. Am J Physiol 279:E927–E940
23. Kaneto H, Xu G, Song KH et al (2001) Activation of the hexosamine pathway leads to deterioration of pancreatic β-cell function through the induction of oxidative stress. J Biol Chem 276:31099–31104
24. Takahashi H, Tran PO, LeRoy E, Harmon JS, Tanaka Y, Robertson RP (2004) D-Glyceraldehyde causes production of intracellular peroxide in pancreatic islets, oxidative stress, and defective beta cell function via non-mitochondrial pathways. J Biol Chem 279:37316–37323
25. Tsubouchi H, Inoguchi T, Inuo M et al (2005) Sulfonylurea as well as elevated glucose levels stimulate reactive oxygen species production in the pancreatic β-cell line, MIN6—a role of NAD(P) H oxidase in β-cells. Biochem Biophys Res Commun 326:60–65
26. Yu BP (1994) Cellular defenses against damage from reactive oxygen species. Physiol Rev 74:139–162
27. Turrens JF (2003) Mitochondrial formation of reactive oxygen species. J Physiol 552:335–344
28. Kadenbach B (2003) Intrinsic and extrinsic uncoupling of oxidative phosphorylation. Biochim Biophys Acta 1604:77–94
29. Ohnishi M, Tokuda M, Masaki T et al (1994) Changes in annexin I and II levels during the postnatal development of rat pancreatic islets. J Cell Sci 107:2117–2125
30. Tejedo JR, Ramirez R, Cahuana GM, Rincon P, Sobrino F, Bedoya FJ (2001) Evidence for involvement of c-Src in the anti-apoptotic action of nitric oxide in serum-deprived RINm5F cells. Cell Signal 13:809–817
31. Tejedo JR, Cahuana GM, Ramirez R et al (2004) Nitric oxide triggers the phosphatidylinositol 3-kinase/Akt survival pathway in insulin-producing RINm5F cells by arousing Src to activate insulin receptor substrate-1. Endocrinology 145:2319–2327
32. Cheng H, Straub SG, Sharp GW (2007) Inhibitory role of Src family tyrosine kinases on Ca^{2+}-dependent insulin release. Am J Physiol 292:E845–E852
33. Roskoski R Jr (2004) Src protein-tyrosine kinase structure and regulation. Biochem Biophys Res Commun 324:1155–1164
34. Haas M, Askari A, Xie Z (2000) Involvement of Src and epidermal growth factor receptor in the signal-transducing function of Na^+/K^+-ATPase. J Biol Chem 275:27832–27837
35. Aydemir-Koksoy A, Abramowitz J, Allen JC (2001) Ouabain-induced signaling and vascular smooth muscle cell proliferation. J Biol Chem 276:46605–46611
36. Haas M, Wang H, Tian J, Xie Z (2002) Src-mediated inter-receptor cross-talk between the Na^+/K^+-ATPase and the epidermal growth factor receptor relays the signal from ouabain to mitogen-activated protein kinases. J Biol Chem 277:18694–18702
37. Xie Z, Cai T (2003) Na^+-K^+-ATPase-mediated signal transduction: from protein interaction to cellular function. Mol Interv 3:157–168
38. Hutton JC, Malaisse WJ (1980) Dynamics of O_2 consumption in rat pancreatic islets. Diabetologia 18:395–405
39. Sener A, Malaisse WJ (1991) Hexose metabolism in pancreatic islets. Regulation of D-[6–^{14}C]glucose oxidation by non-nutrient secretagogues. Mol Cell Endocrinol 76:1–6
40. Nulton-Persson AC, Szweda LI (2001) Modulation of mitochondrial function by hydrogen peroxide. J Biol Chem 276:23357–23361
41. Leahy JL, Bonner-Weir S, Weir GC (1992) Beta-cell dysfunction induced by chronic hyperglycemia. Current ideas on mechanism of impaired glucose-induced insulin secretion. Diabetes Care 15:442–455
42. Kimura K, Toyota T, Kakizaki M, Kudo M, Takebe K, Goto Y (1982) Impaired insulin secretion in the spontaneous diabetes rats. Tohoku J Exp Med 137:453–459
43. Portha B, Serradas P, Bailbe D, Suzuki K, Goto Y, Giroix MH (1991) β-cell insensitivity to glucose in the GK rat, a spontaneous nonobese model for type II diabetes. Diabetes 40:486–491
44. Hughes SJ, Faehling M, Thorneley CW, Proks P, Ashcroft FM, Smith PA (1998) Electrophysiological and metabolic characterization of single β-cells and islets from diabetic GK rats. Diabetes 47:73–81
45. Anello M, Lupi R, Spampinato D et al (2005) Functional and morphological alterations of mitochondria in pancreatic beta cells from type 2 diabetic patients. Diabetologia 48:282–289
46. Ihara Y, Toyokuni S, Uchida K et al (1999) Hyperglycemia causes oxidative stress in pancreatic β-cells of GK rats, a model of type 2 diabetes. Diabetes 48:927–932
47. Sakuraba H, Mizukami H, Yagihashi N, Wada R, Hanyu C, Yagihashi S (2002) Reduced beta-cell mass and expression of oxidative stress-related DNA damage in the islet of Japanese type II diabetic patients. Diabetologia 45:85–96

Dietary Corosolic Acid Ameliorates Obesity and Hepatic Steatosis in KK-Ay Mice

Kotaro YAMADA,[a] Masaya HOSOKAWA,*[,a] Chizumi YAMADA,[a] Rie WATANABE,[a] Shimpei FUJIMOTO,[a] Hideya FUJIWARA,[a] Masaru KUNITOMO,[b] Toshihiro MIURA,[c] Tetsuo KANEKO,[d] Kinsuke TSUDA,[e] Yutaka SEINO,[a,f] and Nobuya INAGAKI[a]

[a] *Department of Diabetes and Clinical Nutrition, Kyoto University Graduate School of Medicine; 54 Shogoin-Kawahara-cho, Sakyo-ku, Kyoto 606–8507, Japan:* [b] *Department of Pharmacology, Faculty of Pharmaceutical Sciences, Mukogawa Women's University; 11–68 Koshien, Kyuban-cho, Nishinomiya 663–8179, Japan:* [c] *Department of Clinical Nutrition, Suzuka University of Medical Science; 1001–1 Kishioka, Suzuka, Mie 510–0293, Japan:* [d] *Department of Pharmaceutical Science, Hiroshima International University; 5–1–1 Hiro-Koshingai, Kure, Hiroshima 737–0112, Japan:* [e] *Laboratory of Metabolism, Graduate School of Human and Environmental Studies, Kyoto University; Yoshida-nihonmatsu-cho, Sakyo-ku, Kyoto 606–8501, Japan: and* [f] *Kansai Electric Power Hospital; Osaka 553–0003, Japan.*

Received November 6, 2007; accepted January 25, 2008; published online January 29, 2008

Corosolic acid (CRA), a constituent of Banaba leaves, has been reported to exert anti-hypertension, anti-hyperinsulinemia, anti-hyperglycemia, and anti-hyperlipidemia effects as well as to induce anti-inflammatory and anti-oxidative activities. The aim of this study was to investigate the inhibitory effects of CRA on the development of obesity and hepatic steatosis in KK-Ay mice, a genetically obese mouse model. Six-week-old KK-Ay mice were fed a high fat diet for 9 weeks with or without 0.023% CRA. Nine-week CRA treatment resulted in 10% lower body weight and 15% lower total fat (visceral plus subcutaneous fat) mass than in control mice. CRA treatment reduced fasting plasma levels of glucose, insulin, and triglyceride by 23%, 41%, and 22%, respectively. The improved insulin sensitivity in CRA-treated mice may be due on part to the increased plasma adiponectin and white adipose tissue (WAT) AdipoR1 levels. In addition, CRA treatment increased the expression of peroxisome proliferator-activated receptor (PPAR)α in liver and PPARγ in WAT. This is the first study to show that CRA treatment can contribute to reduced body weight and amelioration of hepatic steatosis in mice fed a high fat diet, due in part to increased expression of PPARα in liver and PPARγ in WAT.

Key words corosolic acid; peroxisome proliferator-activated receptor; obesity; hepatic steatosis

Banaba leaves (*Lagerstroemia speciosa* LINN.) have been used as a traditional medicine in Southeast Asia, and tea made from the leaves is used as a treatment for diabetes. The leaves contain large amounts of corosolic acid (CRA) (Fig. 1), which recently has attracted attention for its biological properties.[1—7] It was shown that Banaba leaf extract (1% CRA) treatment for 2 weeks decreased blood glucose levels in humans.[8] In addition, CRA (10 mg) has been shown to reduce post challenge plasma glucose levels at 90 min in humans.[7] We previously reported that CRA ameliorates hypertension and abnormal lipid metabolism as well as mitigating oxidative stress and the inflammatory state in SHR/NDmcr-cp rats on a high fat diet,[9] that is an animal model of metabolic syndrome.[10] We also found that the administration of CRA (10 mg/kg) in a normal diet for 2 weeks improved hyperglycemia by reducing insulin resistance in a KK-Ay mouse, an obese animal model that spontaneously develops hypertriglyceridemia, hyperglycemia, hyperinsulinemia, and diabetes.[11,12] However, the effects of CRA on the adipocytokines and transcription factors that play central roles in the development of obesity are unknown.

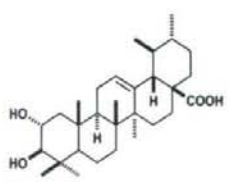

Fig. 1. Structure of Corosoric Acid (CRA)

Obesity and type 2 diabetes in both humans and animals are associated with insulin resistance.[13] Adiponectin is an insulin-sensitizing hormone, and plasma levels of adiponectin have been reported to be significantly reduced in obese /diabetic mice and humans.[14—16] It also was reported that adiponectin receptors, AdipoR1 and AdipoR2, are downregulated in adipose tissue and skeletal muscle in obese diabetic ob/ob mouse, which is correlated with decreased adiponectin sensitivity.[17]

Abnormalities of lipid metabolism are frequently observed in obesity and type 2 diabetes. Peroxisome proliferator-activated receptor (PPAR)α is predominantly expressed in liver, and regulates the expression of genes involved in lipid metabolism. Activators of PPARα decrease circulating lipid levels and are commonly used to treat hypertriglyceridemia and other dyslipidemic states. Recent studies suggest that the activation of PPARα prevents high fat diet-induced obesity,[18] insulin resistance,[18,19] and hepatic steatosis.[20] It was also found that activation of PPARα increased AdipoR1 and AdipoR2 expression in adipocytes *in vivo*.[21]

Growth and differentiation of adipocytes are regulated by PPARγ, which is highly expressed in adipose tissue. Activation of PPARγ by agonists such as thiazolidinediones increases the number of small adipocytes, which increases the amount of the insulin-sensitizing hormone adiponectin.[15,22] PPARγ activation also stimulates lipid storage in adipocytes and reduces lipotoxicity in liver and skeletal muscle, thereby improving insulin sensitivity.[23]

In the present study, we examined the inhibitory effects of CRA on the development of obesity and hepatic steatosis in

* To whom correspondence should be addressed. e-mail: hosokawa@metab.kuhp.kyoto-u.ac.jp

KK-Ay mice using 43 mg/kg CRA, a dosage similar to that used in the previous study.[11] We performed biochemical measurements, body composition analysis, and morphological analysis of liver and white adipose tissue (WAT). In addition, we examined gene and protein expression of PPARα in liver, which regulates β-oxidation of fatty acid. We also examined gene expression of AdipoR1 and AdipoR2, which are increased by PPARα agonist, and PPARα, which increases adiponectin, in WAT.

MATERIALS AND METHODS

Chemicals CRA provided by Use Techno Corporation (Kyoto, Japan) was stored at room temperature until use. All other chemicals were of reagent grade.

Animals Male KK-Ay mice were purchased from Clea Japan (Tokyo, Japan). The mice were housed in an air-controlled room (temperature 25±2 °C and 50% humidity) with a 12 h light/dark-cycle and food and water provided *ad libitum*. Six-week-old male KK-Ay mice (1 mouse/cage) were fed a high fat diet with (CRA-treated mice) or without (control mice) 0.023% (w/w) CRA for 9 weeks. The high fat diet contained 45% kcal as fat, 35% kcal as carbohydrate, and 20% kcal as protein, with an energy density of 3.57 kcal/g.[24] All studies were performed in the laboratories of the Department of Diabetes and Clinical Nutrition, Kyoto University, in accordance with the Declaration of Helsinki. The Animal Care Committee of Kyoto University Graduate School of Medicine approved animal care and procedures.

Computed Tomography (CT)-Based Body Composition Analysis CT-based analysis of body composition was performed after 9 weeks. The mice were anesthetized with intraperitoneal injections of pentobarbital sodium, and scanned using a LaTheta (LCT-100M) experimental animal CT system (Aloka, Tokyo, Japan). Contiguous 1 mm slice images of the whole abdominal cavity (Fig. 3A) were used for quantitative assessment by LaTheta software (version 1.00), as described previously.[25] Visceral plus subcutaneous fat mass (total fat mass) and lean body mass were evaluated quantitatively.

Histological Examination Epididymal white adipose tissue (WAT) after 9 weeks was removed and fixed in 10% formalin, embedded in paraffin, and stained with hematoxylin and eosin.[26] The diameter of the adipocytes was determined by microsocope (BZ-8000, Keyence, Osaka, Japan); 50 cells per mouse were measured in several parts of the epididymal fat pad. Liver was fixed in 4% paraformaldehyde in 0.1 M phosphate-buffered saline for 2 h at 4 °C, frozen, sectioned, stained with Oil Red O, and counterstained with hematoxylin.[27]

Measurement of Liver Triglyceride (TG) Content To analyze hepatic TG levels, approximately 0.2 g of tissue was homogenized and extracted in a chloroform : methanol mixture (2 : 1 v/v).[28] Triglyceride was enzymatically quantified using a TG E Test Wako (Wako Pure Chemical Industries, Osaka, Japan).

Biochemical Measurements Blood samples were collected in heparinized capillary tubes and centrifuged at 2400 ***g***. Plasma TG and glucose levels were measured using a TG E test and Glucose II test, respectively (Wako Pure Chemical Industries, Osaka, Japan). Plasma insulin levels were measured using a mouse insulin ELISA kit (Shibayagi, Gunma, Japan). Plasma adiponectin levels were measured by mouse/rat adiponectin immunoassay kit (Otsuka Pharmaceutical, Tokushima, Japan).

Quantitaive Reverse Transcription-Polymerase Chain Reaction (RT-PCR) Total RNA was isolated from liver and fat with Trizol reagent (Invitrogen, CA, U.S.A.), and examined by real time quantitative RT-PCR using a PE Applied Biosystems prism model 7000 sequence detection instrument. SYBER Green PCR Master Mix (Applied Biosystem, CA, U.S.A.) was prepared for the PCR run. Thermal cycling conditions were denaturation at 95 °C for 10 min followed by 50 cycles at 95 °C for 15 s and 60 °C for 1 min. The sequences of the sense and antisence primers of PPARα, PPARγ, AdipoR1 and AdipoR2 used for amplication from mouse liver and WAT were as follows: the sense primer for PPARα was ccctgaacatcgagtgtcgaa, the antisence primer ttgcagctccgatcacactt; the sense primer for PPARα was tgtcggtttcagaagtgcctt, the antisense primer gctcgcagatcagcagactct; the sense primer for AdipoR1 was 5′-acgttggagagtcatcccgtat-3′, the antisense primer 5′-ctctgtgtggatgcggaagat-3′; the sense primer for AdipoR2 was 5′-tcccaggaagatgaagggtttat-3′, the antisence primer 5′-ttccattcgttcgatagcatga-3′. Gene expression levels were corrected for GAPDH mRNA level.

Protein Analysis For PPARα analysis, nuclear extracts were prepared essentially as described by Gebel *et al.*[29] Briefly, frozen liver samples (0.1 g) were homogenized in 0.5 ml of ice cold buffer containing 20 mM Tris–HCl (pH 7.4), 10% glycerol, 1 mM EDTA, 25 mM KCl, and 1 mM dithiothreitol together with protease inhibitors (Complete, EDTA Free; Roche, Mannheim, Germany), and the nuclei were then pelleted and resuspended in fresh buffer 0.4 M NaCl. The suspensions were mixed (4 °C, 30 min) and centrifuged (2000×***g***, 4 °C, 30 min), and supernatants (nuclear extracts) were collected. Protein was analyzed using a kit from Bio-Rad Laboratories (CA, U.S.A.) with bovine serum albumin as standard.

Nuclear Extracts (15 μg protein) were 12% SDS-polyacrylamide gels, transferred to PVDF membranes, which were blocked in TBST buffer (20 mM Tris–HCl [pH 7.5] and 55 mM NaCl, 0.1% Tween 20) containing 5% non-fat milk powder and incubated with primary antibody 24 h. Primary antibodies and dilutions used were as follows: mouse anti-GAPDH (1 : 5000, Chemicon, CA, U.S.A.), rabbit anti-murine PPARα (1 : 500, Santa Cruz Biothechnology, SantaCruz, CA, U.S.A.). TBST was used as wash buffer and antibody diluent. After washing for 3×10 min, blots were incubated (60 min) with horseradish peroxidase-conjugated secondary anti-bodies, either anti-rabbit IgG (1 : 5000, GE Healthcare, Buckinghamshire, U.K.) or anti-mouse IgG (1 : 5000, GE Healthcare, Buckinghamshire, U.K.). Blots were given final washes (2×15 min) and antibody binding was detected on X-ray film by enhanced chemiluminescenece (ECL Advance, GE Healthcare, Buckinghamshire, U.K.).

Statistics Results are expressed as mean±S.E.M. Statistical analysis was performed using unpaired Student's *t*-test for data from control and CRA-treated mice. Difference was considered significant at $p<0.05$.

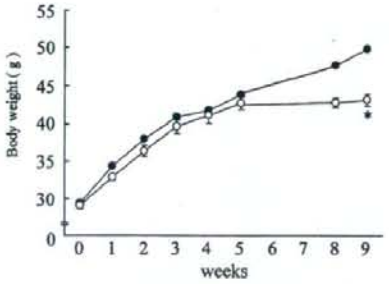

Fig. 2. Body Weight of Control Mice (Closed Circle) and CRA-Treated Mice (Open Circle) During 9-Week Observation Period on a High Fat Diet with or without 0.023% CRA

Each value represents mean±S.E.M. (n=4). Significantly different from controls, *p<0.05.

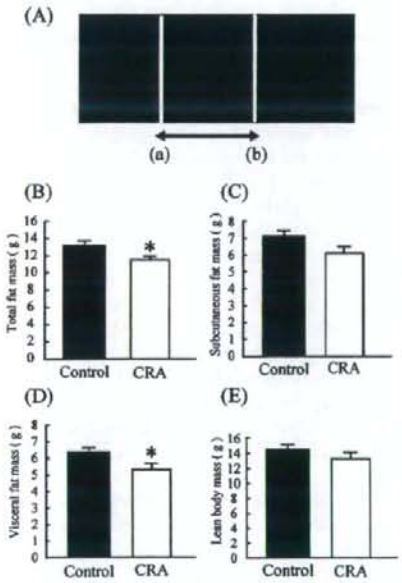

Fig. 3. Computed Tomography (CT)-Based Body Composition Analysis

(A) The arrow (from (a) to (b)) indicates the observation area. (B) total fat mass, (C) subcutaneous fat mass, (D) visceral fat mass, and (E) lean body mass of control mice (closed bar) and CRA-treated mice (CRA) (open bar) after 9 weeks on a high fat diet with or without 0.023% CRA. Each value represents mean±S.E.M. (n=4). Significantly different from controls, *p<0.05.

RESULTS

Effects of CRA on Body Weight and Fat Mass in KK-Ay Mice KK-Ay mice were fed a high fat diet with (CRA-treated mice) or without (control mice) 0.023 % (w/w) CRA for 9 weeks. As shown in Fig. 2, mice treated with CRA for 9 weeks had 10% less body weight than control mice. In normal diet-fed mice, there were no significant differences in CRA-treated or control mice (data not shown). There were no significant differences in food intake between CRA-treated (460±10 g/9 weeks) and control mice (454±8 g/9 weeks). As shown in Fig. 3, a significant decrease in total fat mass (Fig. 3B, 15%, p<0.05) and visceral fat mass (Fig. 3D, 16%, p<0.05) was observed in CRA-treated mice compared

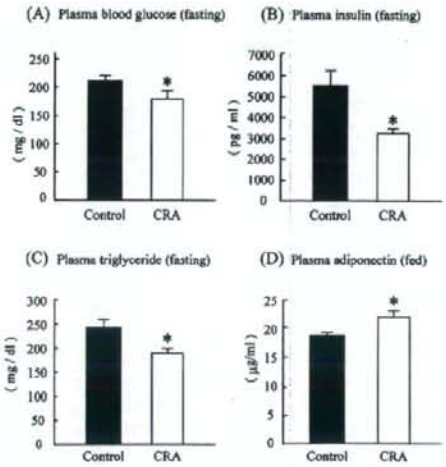

Fig. 4. (A) Fasting Plasma Blood Glucose Levels, (B) Fasting Plasma Insulin Levels, (C) Fasting Plasma Triglyceride Levels, and (D) Fed Plasma Adiponectin Levels of Control Mice (Closed Bar) and CRA-Treated Mice (CRA) (Open Bar) after 9 Weeks on a High Fat Diet with or without 0.023% CRA

Each value represents mean±S.E.M. (n=4). Significantly different from controls, *p<0.05.

to controls. Subcutaneous fat mass was somewhat decreased, but not significantly, in the CRA-treated mice (Fig. 3C, 14%, p<0.09). Lean body mass was similar in control and CRA-treated mice (Fig. 3E).

Effects of CRA on Fasting Plasma Glucose, Insulin, TG and Fed Plasma Adiponectin Levels As shown in Fig. 4, the CRA-treated mice showed levels of fasting plasma glucose (A) and insulin (B) reduced by 23% (p<0.05) and 41% (p<0.05), respectively, compared to controls, suggesting that the CRA-treated mice were more insulin sensitive. CRA-treated mice showed fasting plasma TG (Fig. 4C) levels reduced by 22% (p<0.05) compared to controls. Fed plasma levels of adiponectin were higher (16%, p<0.05) in CRA-treated mice compared to controls (Fig. 4D).

Histology of Epididymal WAT and Effects of CRA on WAT mRNA Expression Levels of AdipoR1, AdipoR2 and PPARγ Figure 5A shows representative sections of epididymal WAT from control and mice treated with CRA for 9 weeks, stained with hematoxylin and eosin. As shown in Fig. 5B, the size of adipocytes of epididymal WAT of CRA-treated mice was significantly less (28%, p<0.05) than that of controls. AdipoR1 mRNA expression levels were significantly higher in CRA-treated mice (15%, p<0.05) than in controls (Fig. 5C), although there was no difference in AdipoR2 mRNA between control and CRA-treated mice (Fig. 5D). CRA-treated mice showed significantly elevated PPARγ mRNA expression levels (60%, p<0.05) compared to controls (Fig. 5E).

Histology of Liver, Liver TG Content, and Hepatic mRNA and Protein Expression of PPARα Figure 6A shows Oil Red O-stained sections of liver of control mice and CRA-treated mice. The liver of control mice showed widespread deposition of fat globules of various sizes. In contrast, the liver of CRA-treated mice showed less fat accumulation, indicating less hepatic steatosis than in controls.

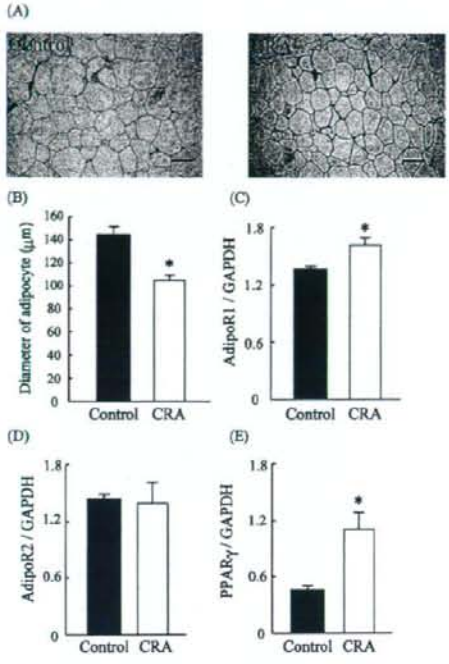

Fig. 5. (A) Histology of Epididymal White Adipose Tissue (WAT) of Control and CRA-Treated Mice (CRA) after 9 Weeks on a High Fat Diet with or without 0.023% CRA

Original magnification: 200×. Scale bars: 100 μm.

(B) Diameter of Adipocytes in Epididymal Fat Pad of Control Mice (Closed Bar) and CRA-Treated Mice (CRA) (Open Bar) after 9 Weeks on a High Fat Diet with or without 0.023% CRA and Quantitative Real-Time RT-PCR Analysis of Fatty Expression of (C) AdipoR1, (D) AdipoR2 and (E) PPARγ mRNA of Control Mice (Closed Bar) and CRA-Rreated Mice (CRA) (Open Bar) after 9 Weeks on a High Fat Diet with or without 0.023% CRA

Gene expression levels of each mRNA were corrected for GAPDH mRNA levels. Each value represents mean±S.E.M. (n=4). Significantly different from controls, *p<0.05.

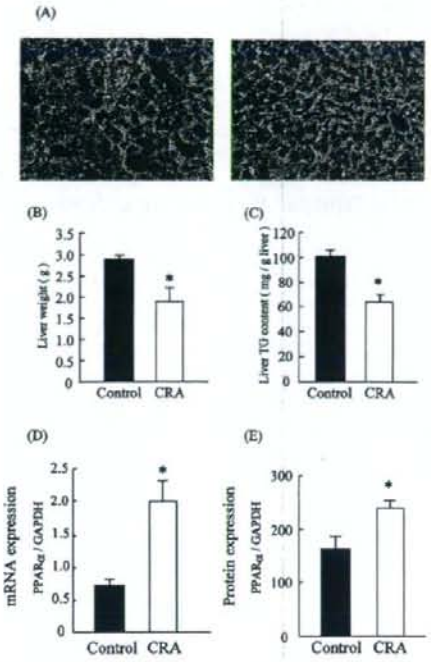

Fig. 6. (A) Photomicrographs of Oil Red O Stained Liver of Control and CRA-Treated Mice (CRA) after 9 Weeks on a High Fat Diet with or without 0.023% CRA

Original magnification: 100×. Scale bars: 200 μm.

(B) Liver Weight of Control Mice (Closed Bar) and CRA-Treated Mice (CRA) (Open Bar) after 9 Weeks on a High Fat Diet with or without 0.023% CRA, (C) Liver TG Content of Control Mice (Closed Nar) and CRA-Treated Mice (CRA) (Open Bar) after 9 Weeks on a High Fat Diet with or without 0.023% CRA, Quantitative Real-Time RT-PCR Analyses of Hepatic (D) mRNA Expression and (E) Protein Expression of PPARα of Control Mice (Closed Bar) and CRA-Treated Mice (CRA) (Open Bar) after 9 Weeks on High Fat Diet with or without 0.023% CRA

Gene and protein expression levels of PPARα were corrected for GAPDH levels. Each value represents mean±S.E.M. (n=4). Significantly different from controls, *p<0.05.

The liver weight of CRA-treated mice was significantly less (35%, p<0.05) than in controls (Fig. 6B), which is associated with the significantly decreased hepatic TG accumulation in CRA-treated mice (37%, p<0.05) (Fig. 6C). Since PPARα plays an important role in maintaining homeostasis of lipid metabolism, PPARα mRNA expression was examined in liver samples from controls and mice treated with CRA for 9 weeks. As shown in Fig. 6D, expression of PPARα mRNA in CRA-treated mice was significantly higher (64%, p<0.05) than in controls. We also confirmed protein expression of PPARα and found that CRA-treated mice showed significantly higher (31%, p<0.05) PPARα protein levels than in controls (Fig. 6E).

DISCUSSION

This is the first study to show that CRA treatment in mice fed a high fat diet contributes to reduced body weight and hepatic steatosis associated with increased expression of PPARα in liver and PPARγ in WAT. CRA treatment also may improve insulin sensitivity by increasing plasma adiponectin and WAT AdipoR1 levels.

In the present study, we found that CRA increased mRNA and protein expression of PPARα in liver, suggesting that CRA may act as a PPARα agonist. The decreased body weight and fat mass observed in the CRA-treated mice are most likely due to increased β-oxidation and energy expenditure by PPARα activation, as seen in mice treated with PPARα agonists.[18,19,30,31] Hypertriglycemia and hepatic steatosis are also ameliorated by CRA treatment, in a manner similar to that by PPARα agonists,[20] by increasing fatty acid β-oxidation in liver. CRA-treated mice on a high fat diet showed significantly reduced liver weight compared to controls, due to the significantly decreased hepatic TG accumulation. However, there are several reports of increased liver weight by synthetic PPARα agonists in rodents on a normal diet[32–34] through induction of DNA synthesis and suppression of apoptosis in hepatocytes.[35] In the present study, increased AdipoR1 expression in WAT was found in the CRA-treated mice, which may well contribute partly to the CRA-related improvement in insulin sensitivity.

In addition, CRA treatment was found in the present study

to increase PPARγ expression in WAT. Treatment of obese diabetic mice with thiazolidinediones, a PPARγ agonist, has been suggested to stimulate adipocyte differentiation and apoptosis, thereby preventing adipocyte hypertrophy,[23,36] which is consistent with our results. Increased plasma adiponectin levels also play an essential role in improved insulin sensitivity in CRA-treated mice, most likely due to increased number of small adipocytes through CRA-induced activation of PPARγ in WAT, resulting in decreased plasma glucose levels.

It is noteworthy that CRA can activate both PPARα and PPARγ. Tsuchida *et al.* reported that activation of PPARα and PPARγ by combination therapy of Wy-14643 and rosiglitazone improved insulin sensitivity and reduced body weight in KK-Ay mice.[21] Compounds that have dual agonistic activity on both of these receptors have been shown to exhibit several beneficial metabolic effects in obese diabetic animals. Ragaglitazar, a PPARα and PPARγ agonist, was shown to reduce plasma TG and glucose levels in high fat diet-fed animals in the absence of weight gain,[32] and similar results were obtained in Zucker *fa/fa* rats.[37] CRA may therefore have therapeutic potential as a dual agonist of PPARα and PPARγ.

In conclusion, we have demonstrated that CRA ameliorates high fat diet-induced obesity and hepatic steatosis in genetically obese KK-Ay mice, at least in part, by increasing PPARα expression in liver and PPARγ expression in WAT. CRA treatment also improved insulin sensitivity by increasing plasma adiponectin levels and WAT AdipoR1 levels. As obese patients are likely to prefer a high fat diet, CRA may be an effective therapeutic option for the treatment of obesity and diabetes.

Acknowledgments This study was supported by Scientific Research Grants and Grant-in-Aid for Creative Scientific Research (15GS0301) from the Ministry of Education, Culture, Sports, Science and Technology of Japan.

REFERENCES

1) Murakami C., Myoga K., Kasai R., Ohtani K., Kurokawa T., Ishibashi S., Dayrit F., Padolina W. G., Yamasaki K., *Chem. Pharm. Bull.*, **41**, 2129—2131 (1993).
2) Ahn K. S., Hahm M. S., Park E. J., Lee H. K., Kim I. H., *Planta Med.*, **64**, 468—470 (1998).
3) Miura T., Itoh Y., Kaneko T., Ueda N., Ishida T., Fukushima M., Matsuyama F., Seino Y., *Biol. Pharm. Bull.*, **27**, 1103—1105 (2004).
4) Dat N. T., Cai X. F., Rho M. C., Lee H. S., Ba K., Kim Y. H., *Arch. Pharm. Res.*, **28**, 164—168 (2005).
5) Kim D. H., Han K. M., Chung I. S., Kim D. K., Kim S. H., Kwon B. M., Jeong T. S., Park M. H., Ahn E. M., Baek N. I., *Arch. Pharm. Res.*, **28**, 550—556 (2005).
6) Wen X., Sun H., Liu J., Wu G., Zhang L., Wu X., Ni P., *Bioorg. Med. Chem. Lett.*, **15**, 4944—4948 (2005).
7) Fukushima M., Matsuyama F., Ueda N., Egawa K., Takemoto J., Kajimoto Y., Yonaha N., Miura T., Kaneko T., Nishi Y., Mitsui R., Fijita Y., Yamada Y., Seino Y., *Diabetes Res. Clin. Pract.*, **73**, 174—177 (2006).
8) Judy W. V., Hari S. P., Stogsdill W. W., Judy J. S., Naguib Y. M., Passwater R., *J. Ethnopharmacol.*, **87**, 115—117 (2003).
9) Yamaguchi Y., Yamada K., Yoshikawa N., Nakamura K., Haginaka J., Kunitomo M., *Life Sci.*, **79**, 2474—2479 (2006).
10) Nangaku M., Miyata T., Sada T., Mizuno M., Inagi R., Ueda Y., Ishikawa N., Yuzawa H., Koike H., van Ypersele de Strihou C., Kurokawa K., *J. Am. Soc. Nephrol.*, **14**, 1212—1222 (2003).
11) Miura T., Ueda N., Yamada K., Fukushima M., Ishida T., Kaneko T., Matsuyama F., Seino Y., *Biol. Pharm. Bull.*, **29**, 585—587 (2006).
12) Fujita T., Sugiyama Y., Taketomi S., Sohda T., Kawamatsu Y., Iwatsuka H., Suzuoki Z., *Diabetes*, **32**, 804—810 (1983).
13) Boden G., *Diabetes*, **46**, 3—10 (1997).
14) Hu E., Liang P., Spiegelman B. M., *J. Biol. Chem.*, **271**, 10697—10703 (1996).
15) Yamauchi T., Kamon J., Waki H., Terauchi Y., Kubota N., Hara K., Mori Y., Ide T., Murakami K., Tsuboyama-Kasaoka N., Ezaki O., Akanuma Y., Gavrilova O., Vinson C., Reitman M. L., Kagechika H., Shudo K., Yoda M., Nakano Y., Tobe K., Nagai R., Kimura S., Tomita M., Froguel P., Kadowaki T., *Nat. Med.*, **7**, 941—946 (2001).
16) Arita Y., Kihara S., Ouchi N., Takahashi M., Maeda K., Miyagawa J., Hotta K., Shimomura I., Nakamura T., Miyaoka K., Kuriyama H., Nishida M., Yamashita S., Okubo K., Matsubara K., Muraguchi M., Ohmoto Y., Funahashi T., Matsuzawa Y., *Biochem. Biophys. Res. Commun.*, **257**, 79—83 (1999).
17) Tsuchida A., Yamauchi T., Ito Y., Hada Y., Maki T., Takekawa S., Kamon J., Kobayashi M., Suzuki R., Hara K., Kubota N., Terauchi Y., Froguel P., Nakae J., Kasuga M., Accili D., Tobe K., Ueki K., Nagai R., Kadowaki T., *J. Biol. Chem.*, **279**, 30817—30822 (2004).
18) Guerre-Millo M., Gervois P., Raspe E., Madsen L., Poulain P., Derudas B., Herbert J. M., Winegar D. A., Willson T. M., Fruchart J. C., Berge R. K., Staels B., *J. Biol. Chem.*, **275**, 16638—16642 (2000).
19) Ye J. M., Doyle P. J., Iglesias M. A., Watson D. G., Cooney G. J., Kraegen E. W., *Diabetes*, **50**, 411—417 (2001).
20) Lee G. Y., Kim N. H., Zhao Z. S., Cha B. S., Kim Y. S., *Biochem. J.*, **378**, 983—990 (2004).
21) Tsuchida A., Yamauchi T., Takekawa S., Hada Y., Ito Y., Maki T., Kadowaki T., *Diabetes*, **54**, 3358—3370 (2005).
22) Yamauchi T., Waki H., Kamon J., Murakami K., Motojima K., Komeda K., Miki H., Kubota N., Terauchi Y., Tsuchida A., Tsuboyama-Kasaoka N., Yamauchi N., Ide T., Hori W., Kato S., Fukayama M., Akanuma Y., Ezaki O., Itai A., Nagai R., Kimura S., Tobe K., Kagechika H., Shudo K., Kadowaki T., *J. Clin. Invest.*, **108**, 1001—1013 (2001).
23) Yamauchi T., Kamon J., Waki H., Murakami K., Motojima K., Komeda K., Ide T., Kubota N., Terauchi Y., Tobe K., Miki H., Tsuchida A., Akanuma Y., Nagai R., Kimura S., Kadowaki T., *J. Biol. Chem.*, **276**, 41245—41254 (2001).
24) Miyawaki K.,Yamada Y., Yano H., Niwa H., Ban N., Ihara Y., Kubota A., Fujimoto S., Kajikawa M., Kuroe A., Tsuda K., Hashimoto H., Yamashita T., Jomori T., Tashiro F., Miyazaki J., Seino Y., *Proc. Natl. Acad. Sci. U.S.A.*, **96**, 14843—14847 (1999).
25) Yamada C., Yamada Y., Tsukiyama K., Yamada K., Yamane S., Harada N., Miyawaki K., Seino Y., Inagaki N., *Biochem. Biophys. Res. Commun.*, **364**, 175—180 (2007).
26) Yamada K., Hosokawa M., Fujimoto S., Nagashima K., Fukuda K., Fujiwara H., Ogawa E., Fujita Y., Ueda N., Matsuyama F., Yamada Y., Seino Y., Inagaki N., *Diabetes Res. Clin. Pract.*, **75**, 127—134 (2007).
27) Steneberg P., Rubins N., Bartoov-Shifman R., Walker M. D., Edlund H., *Cell Metab.*, **1**, 245—258 (2005).
28) Carr T. P., Andresen C. J., Rudel L. L., *Clin. Biochem.*, **26**, 39—42 (1993).
29) Gebel T., Arand M., Oesch F., *FEBS Lett.*, **309**, 37—40 (1992).
30) Lee H. J., Choi S. S., Park M. K., An Y. J., Seo S. Y., Kim M. C., Hong S. H., Hwang T. H., Kang D. Y., Garber A. J., Kim D. K., *Biochem. Biophys. Res. Commun.*, **296**, 293—299 (2002).
31) Chou C. J., Haluzik M., Gregory C., Dietz K. R., Vinson C., *J. Biol. Chem.*, **277**, 24484—24489 (2002).
32) Ye J. M., Iglesias M. A., Watson D. G., Ellis B., Wood L., Jensen P. B., Sorensen R. V., Larsen P. J., Cooney G. J., Wassermann K., Kraegen E. W., *Am. J. Physiol. Endocrinol. Metab.*, **284**, E531—E540 (2003).
33) Ameen C., Edvardsson U., Ljungberg A., Asp L., Akerblad P., Tuneld A., Olofsson S. O., Linden D., Oscarsson J., *J. Biol. Chem.*, **280**, 1224—1229 (2005).
34) Larsen P. J., Jensen P. B., Sorensen R. V., Larsen L. K., Vrang N., WulffE. M., Wassermann K., *Diabetes*, **52**, 2249—2259 (2003).
35) Chevalier S., Roberts R. A., *Oncol. Rep.*, **5**, 1319—1327 (1998).
36) Kubota N., Terauchi Y., Miki H., Tamemoto H., Yamauchi T., Komeda K., Satoh S., Nakano R., Ishii C., Sugiyama T., Eto K., Tsubamoto Y., Okuno A., Murakami K., Sekihara H., Hasegawa G., Naito M., Toyoshima Y., Tanaka S., Shiota K., Kitamura T., Fujita T., Ezaki O., Aizawa S., Kadowaki T., *Mol. Cell*, **4**, 597—609 (1999).
37) Chakrabarti R., Vikramadithyan R. K., Misra P., Hiriyan J., Raichur S., Damarla R. K., Gershome C., Suresh J., Rajagopalan R., *Br. J. Pharmacol.*, **140**, 527—537 (2003).

ELSEVIER

Atherosclerosis 198 (2008) 272–279

ATHEROSCLEROSIS

www.elsevier.com/locate/atherosclerosis

Lectin-like oxidized LDL receptor-1 (LOX-1) acts as a receptor for remnant-like lipoprotein particles (RLPs) and mediates RLP-induced migration of vascular smooth muscle cells

Yo Aramaki [b], Hirokazu Mitsuoka [a], Masako Toyohara [a], Toshikazu Jinnai [a], Kazushi Kanatani [c], Katsuyuki Nakajima [c], Eri Mukai [b], Yuichiro Yamada [b,d], Toru Kita [a], Nobuya Inagaki [b], Noriaki Kume [a,*]

[a] *Department of Cardiovascular Medicine, Graduate School of Medicine, Kyoto University, Japan*
[b] *Department of Diabetes and Clinical Nutrition, Graduate School of Medicine, Kyoto University, Japan*
[c] *JIMRO, Co Ltd, Japan*
[d] *Divison of Endocrinology, Diabetes and Geriatric Medicine, Department of Internal Medicine, Akita University School of Medicine, 1-1-1 Hondo, Akita 010-8543, Japan*

Received 22 March 2007; received in revised form 5 December 2007; accepted 15 December 2007
Available online 20 February 2008

Abstract

Objective: Remnant-like lipoprotein particles (RLPs) have been implicated in atherogenesis especially by diabetic dyslipidemia; however, their receptor(s) and effects on vascular smooth muscle cells (VSMCs) remain unclear. In this study, we examined if lectin-like oxidized LDL receptor-1 (LOX-1) acts as a receptor for RLPs and its biological effects in VSMCs.

Methods and results: RLPs were isolated from human plasma by immunoaffinity gel containing anti-apolipoprotein A-I and anti-apolipoprotein B-100 monoclonal antibodies. DiI-labeled RLPs were taken up by CHO-K1 cells stably expressing LOX-1 but not by wild-type CHO-K1 cells. RLPs induced LOX-1 expression and cell migration in bovine VSMCs (BVSMCs), which were significantly suppressed by transfection with LOX-1 specific siRNAs. Inhibitors of metalloproteinases, epidermal growth factor (EGF) receptor tyrosine kinase, heparin-binding EGF-like growth factor (HB-EGF), p38 mitogen-activated protein kinase (p38 MAPK), MAPK kinase (MEK1) and phosphoinositide 3-kinase (PI3K) significantly blocked RLP-induced LOX-1 expression and cell migration of BVSMCs.

Conclusions: The present study provides direct evidence that LOX-1 is a novel receptor for RLPs in VSMCs. LOX-1-mediated uptake of RLPs may thus play important roles in atherogenesis by inducing LOX-1 expression and VSMC migration especially in the settings of postprandial hyperlipidemia, diabetes and metabolic syndrome.

Keywords: LOX-1; Atherosclerosis; Remnant lipoproteins; Vascular smooth muscle; Diabetes mellitus

1. Introduction

Coronary heart disease (CHD) is prevalent in diabetes mellitus and metabolic syndrome [1,2], in which plasma lipoprotein profiles are characterized by elevated remnant lipoprotein levels. Plasma remnant lipoprotein levels have been assessed as levels of remnant-like lipoprotein particles (RLPs) by isolating fractions unbound to two monocolonal antibodies directed to apolipoprotein B-100 and apolipoprotein A-I [3]. By this method, plasma RLP levels have been shown to predict the CHD risk [4–7], and also to have biological effects on macrophages and vascular cells related to atherogenesis [8–11].

Vascular smooth muscle cells (VSMCs) migration from media to intima and subsequent proliferation play key roles in atherogenesis [12]. A previous report has demonstrated

* Corresponding author at: Department of Cardiovascular Medicine, Graduate School of Medicine, Kyoto University, 54 Kawahara-cho, Shogoin, Sakyo-ku, Kyoto 606-8507, Japan. Tel.: +81 75 751 3623; fax: +81 75 751 4094.
E-mail address: nkume@kuhp.kyoto-u.ac.jp (N. Kume).

0021-9150/$ – see front matter © 2008 Elsevier Ireland Ltd. All rights reserved.
doi:10.1016/j.atherosclerosis.2007.12.017

that RLPs induce VSMC proliferation [9]; however, their effects on VSMC migration have not been clarified. In addition, receptors for RLPs in VSMCs have not yet been well characterized, although LRP in the liver [13], apoB-48-R in macrophages [10,14], and VLDL receptor in heart, skeletal muscle, adipose tissue, brain and macrophages [15] have been shown to act as a receptor for RLPs.

Lectin-like oxidized LDL receptor-1 (LOX-1) is a receptor for Ox-LDL expressed in vascular endothelial cells, macrophages and VSMCs [16–21]. LOX-1 expression is dynamically inducible by various proatherogenic stimuli, including tumor necrosis factor-α (TNF-α) [18,21], heparin-binding epidermal growth factor-like growth factor (HB-EGF), [22] and Ox-LDL [23]. Furthermore, LOX-1 is highly expressed by macrophages and VSMCs accumulated in the intima of advanced atherosclerotic lesions, as well as endothelial cells covering early atherosclerotic lesions in vivo [24], indicating that LOX-1 appears to play important roles at various stages of atherogenesis.

In previous reports, LOX-1 has been indicated to act as a receptor for RLPs in vascular endothelial cells using an anti-LOX-1 antibody and an antisense oligonucleotide directed to LOX-1 [25,26]. In the present study, we provide direct evidence, by cDNA and short interference RNAs (siRNAs) transfection, that LOX-1 acts as a receptor for RLP and whereby induce VSMC migration, depending upon HB-EGF shedding and the downstream signal transduction cascades.

2. Materials and methods

2.1. Reagents

AG1478, PD98059, SB203580 and wortmannin were purchased from Calbiochem (San Diego, CA). CRM197 was from Sigma Chemical CO (St. Louis, MO). GM6001 and its negative control compound were from Chemicon (Temecula, CA). PDGF-BB and TNF-α were purchased from Roche (Mannheim, Germany).

2.2. Cell culture

Chinese hamster ovary-K1 (CHO-K1) cells stably expressing human LOX-1 (hLOX-1-CHO) or bovine LOX-1 (bLOX-1-CHO), as well as wild-type CHO-K1 cells (wt-CHO), were established and cultured as previously reported [16,17]. Bovine VSMCs (BVSMCs) were purchased from Cell Applications, Inc. (San Diego, CA) and cultured as previously reported [19,22].

2.3. Antibodies

Mouse anti-bovine LOX-1 and anti-human LOX-1 monoclonal antibodies were prepared by immunization with recombinant bovine and human LOX-1 extracelluler domains as previously described [16]. Polyclonal antibodies for phosphorylated and total SAPK/JNK and p38 MAPK were purchased from Cell Signaling Technology (New England Biolabs, London, UK). Polyclonal antibodies for phosphorylated and total ERK, Akt and EGFR were from Santa Cruz Biotechnology (Santa Cruz, CA).

2.4. Lipoprotein preparation

RLPs and nascent VLDL were separated using an immunoaffinity mixed gel (JIMRO, Gunma, Japan) from triglyceride-rich lipoprotein fraction ($d < 1.006$ g/ml) isolated from human plasma using ultracentrifugation as described previously [3]. LDL fraction ($d = 1.019–1.063$ g/ml) was also isolated and modified oxidatively as previously described [16,17,19]. Lipoproteins were dialyzed overnight against PBS containing 1 mM EDTA (pH 7.4) and sterilized with a 0.22-μm filter unit (Millipore, Billerica, MA). Labeling of lipoproteins with 1,1′-dioctadecyl-3,3,3′,3′-tetramethylindocarbocyanine perchlorate (DiI; Molecular Probes, Eugene, OR) and quantification of DiI-labeled lipoprotein uptake were performed as previously described [16].

2.5. Immunoblot analysis

Total cell lysates were separated on 12% SDS-PAGE, transferred onto nitrocellulose membranes (Schleicher & Schuell, Dassel, Germany) and proved with each primary antibody, horseradish peroxidase-linked secondary antibodies (Amersham, Hilleroed, Denmark) and the ECL Western blotting detection reagents (Amersham). Representative results from three independent experiments are shown in figures.

2.6. Northern blot analysis

Total cellular RNA was isolated by RNeasy Plus Mini Kit (Qiagen, Valencia, CA). Total RNA (15 μg) was subjected to electrophoresis through 1% agarose gels containing formaldehyde, and transferred onto nitrocellulose membranes (OPTITRAN, Schleicher & Schuell). Membranes were hybridized with XhoI fragment of bovine LOX-1 cDNA which had been labeled with [α-^{32}P] dCTP (Amersham) using random oligonucleotide primers (Megaprime DNA labelling systems, Amersham).

2.7. Transwell migration assay

Transwell migration assay was performed as previously described [27,28]. BVSMCs were applied to the upper chamber of transwell (Costar, Corning Inc. Corning, NY) containing serum-free medium and allowed to migrate to lower chamber containing test stimuli through a fibronectin-coated polycarbonate filter (8 μm pore). Migrated cells on the bottom side of filter were fixed with 100% methanol, stained with Harris hematoxylin solution, and counted manually in randomly chosen five high power fields in each tran-

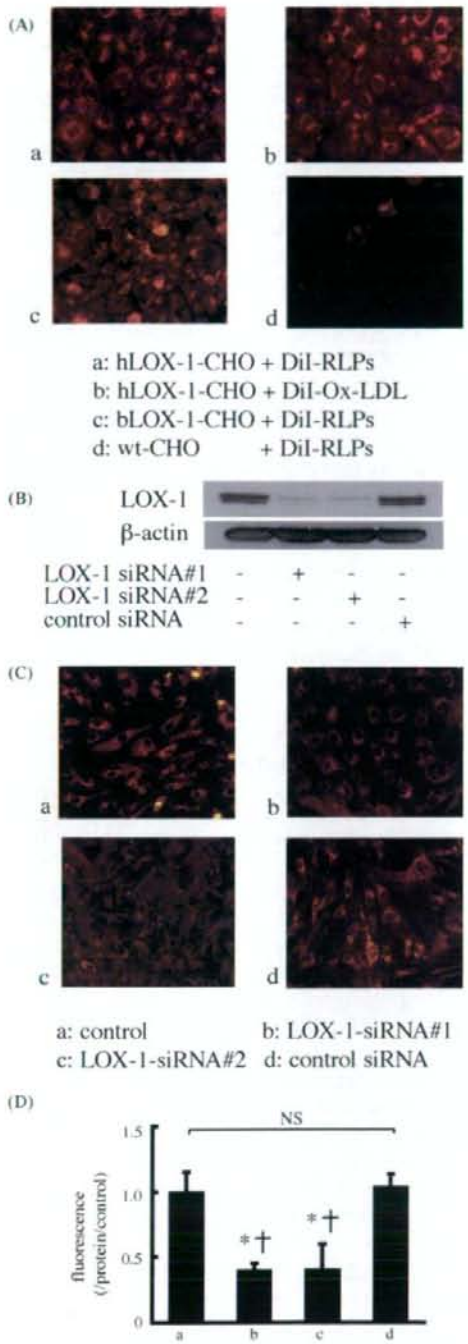

Fig. 1. Human and bovine LOX-1 mediates uptake of RLPs. (A) hLOX-1-CHO were incubated with 5 μg/ml of DiI-RLPs (a) or DiI-labeled Ox-LDL (b) for 2 h. bLOX-1-CHO (c) as well as wt-CHO (d) were incubated with 5 μg/ml of DiI-RLPs. (B) Total cell lysates of bLOX-1-CHO transfected with or without 100 nM of LOX-1 siRNA #1, #2 or control non-silencing siRNA were subjected to Western blotting for LOX-1. (C) BVSMCs (control siRNA) transfected with or without (a) 100 nM of LOX-1 siRNA#1 (b), #2 (c) or control siRNA (d) were incubated with 5 μg/ml of DiI-RLPs. Representative pictures under fluorescence microscopy are shown. (D) Uptake of DiI-RLPs was quantified by measuring fluorescence counts after extraction of DiI. (*) $p < 0.0001$ vs. control, (†) $p < 0.0001$ vs. control siRNA.

swell, using a light microscope (Axioskop2 plus, Zeiss, Jena, Germany). Relative average numbers of migrated BVSMCs compared with the control were calculated.

2.8. LOX-1 specific short interference RNAs (siRNAs)

To block bovine LOX-1 expression, we designed two different siRNAs directed to the coding sequence of bovine LOX-1; siRNA #1: ACCCAAUUACUCGUGGCUU (650-668) and siRNA #2: GGCGAAUCUAUUGAGAGCA (821-839). None of these siRNAs shares homology with exons of other known bovine genes. Control non-silencing siRNA (control siRNA) was obtained from Qiagen. For siRNA transfection, bLOX-1-CHO and BVSMCs were transfected with siRNAs using siFECTOR (B-Bridge International, Inc. Mountain View, CA) according to the manufacturer's instructions.

2.9. Statistical analysis

Data in the bar graphs indicate the mean ± S.D. calculated from three independent experiments. One-way ANOVA was used to compare differences among groups. Statistical significance was defined as $p < 0.05$.

3. Results

3.1. Uptake of DiI-labeled RLPs in CHO-K1 cells stably expressing LOX-1

To examine whether LOX-1 acts as a receptor for RLPs, hLOX-1-CHO, bLOX-1-CHO and wt-CHO were incubated with DiI-labeled RLPs (DiI-RLPs) or DiI-Ox-LDL. As shown in Fig. 1A, hLOX-1-CHO, but not wt-CHO, showed prominent uptake of DiI-RLPs as well as DiI-Ox-LDL. Uptake of DiI-RLP in hLOX-1-CHO was competitively inhibited by the 100-fold excess amount of unlabeled RLPs or Ox-LDL (data not shown), suggesting that uptake of RLPs is specific and that binding sites for RLPs and Ox-LDL on the LOX-1 molecule are identical or overlapped. DiI-RLPs, as well as DiI-Ox-LDL, were also taken up by bLOX-1-CHO. These results thus demonstrate that both human and bovine LOX-1 act as receptors for RLPs.

3.2. Uptake of RLPs by BVSMCs is significantly suppressed by transfection with LOX-1 specific siRNAs

We confirmed that both of LOX-1 siRNA #1 and #2, but not control siRNA, dramatically reduce LOX-1 expression in

bLOX-1-CHO or BVSMCs by more than 90% (Fig. 1B). To determine whether RLPs are mainly taken up by BVSMCs via LOX-1, BVSMCs were incubated with DiI-RLPs after transfection with LOX-1 siRNAs or control siRNA. Uptake of RLPs was significantly reduced in BVSMCs transfected with LOX-1 siRNAs when compared to those transfected with control siRNA or without siRNA (Fig. 1C and D), indicating that LOX-1 is one of major receptors for RLPs in BVSMCs.

3.3. RLPs induce LOX-1 expression in BVSMCs

To explore biological effects of RLPs on BVSMCs, LOX-1 expression was evaluated by Western blotting. As shown in Fig. 2A, treatment of BVSMCs with RLPs, as well as TNF-α, significantly increased LOX-1 expression in a concentration-dependent fashion; maximal effects were observed at 25–50 μg/ml of RLPs. Time-course experiments showed that expression of LOX-1 peaked at 16–20 h after RLP treatment and declined after 24 h (Fig. 2B). Furthermore, Northern blot analyses show RLPs induced LOX-1 expression at the level of gene transcription (Fig. 2C). In contrast with RLPs, nascent VLDL (n-VLDL) had negligible effects on LOX-1 expression in BVSMCs (supplemental Fig. S-A).

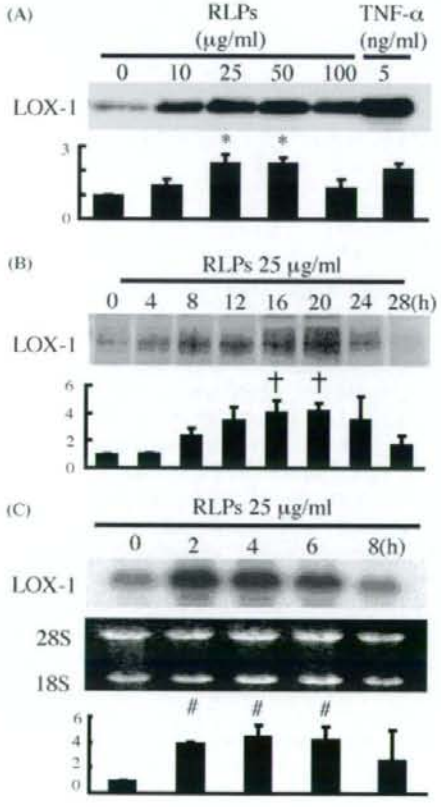

Fig. 2. RLPs, but not nascent VLDL (n-VLDL), induce LOX-1 expression in BVSMCs. (A and B) After BVSMCs were treated with the indicated concentrations of RLPs for 16 h (A) or 25 μg/ml of RLPs for the indicated time periods (B), total cell lysates were subjected to immunoblotting for LOX-1. TNF-α served as a positive control. (C) After treatment with 25 μg/ml of RLPs for the indicated time periods, total cellular RNA was subjected to Northern blot analyses. Bands for 28S and 18S ribosomal RNAs were visualized by ethidium bromide staining to control the amount of RNA loaded. (*) $p < 0.001$ vs. 0 μg/ml of RLPs, (†) $p < 0.005$ vs. 0 h-incubation, (#) $p < 0.05$ vs. 0 h-incubation.

3.4. RLPs induce migration of BVSMCs via LOX-1

Effects of RLPs on BVSMC migration were examined by a transwell migration assay. As shown in Fig. 3A and B, RLPs, as well as PDGF-BB, significantly enhanced BVSMC migration compared with control in serum-free media. N-VLDL showed modest and statistically insignificant increases in BVSMC migration. Statistically significant increases in cell migration were observed at 25 and 50 μg/ml of RLPs after the stimulation for more than 8 h (supplemental Fig. S-B). BVSMC migration was not enhanced when RLPs were present both in the upper and lower chambers, as compared with that without RLPs (supplemental Fig. S-C). Therefore, the increases in the cell numbers on the bottom sides of the filters were due to chemotaxis or cell migration rather than chemokinesis or cell proliferation. Fig. 3C shows that RLP-induced BVSMC migration, but not PDGF-BB-induced BVSMC migration, was significantly inhibited by LOX-1 siRNA transfection. These results indicate LOX-1 mediates RLP-induced BVSMC migration.

3.5. RLP-induced expression of LOX-1 depends upon HB-EGF shedding and EGFR phosphorylation

A previous study has shown that RLPs induce proliferation of rat VSMCs via shedding of HB-EGF and subsequent EGFR transactivation [9], we sought to determine if RLP-induced LOX-1 expression depends upon HB-EGF shedding and EGFR transactivation. As shown in Fig. 4A, RLPs, but not n-VLDL, activate EGFR. In addition, CRM197, which functionally neutralizes HB-EGF, suppressed the activation of EGFR. Furthermore, a metalloproteinase inhibitor GM6001 (GM), but not its negative control compound (GMNC), significantly suppressed RLP-induced LOX-1 expression (Fig. 4B). In addition, AG1478, an EGFR tyrosine kinase inhibitor and CRM197 significantly inhibited LOX-1 expression induced by RLPs, respectively (Fig. 4C and D), indicating involvement of certain metalloproteinases, HB-EGF shedding and transactivation of EGFR in RLP-induced LOX-1 expression in BVSMCs.

3.6. RLP-induced expression of LOX-1 depends upon ERK, p38 MAPK and PI3K activation

To determine which signal transduction cascades are involved in RLP-induced LOX-1 expression in BVSMCs, phosphorylation of ERK, p38 MAPK, c-Jun N-terminal

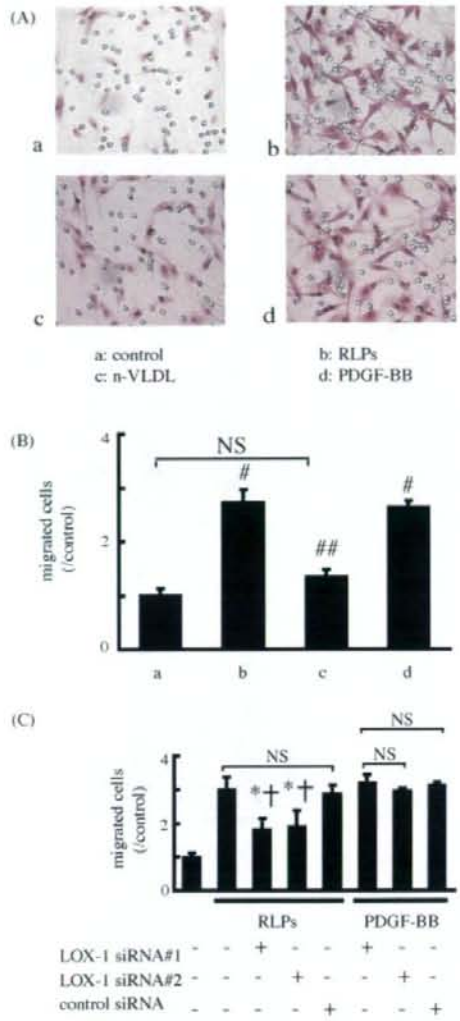

Fig. 3. LOX-1 mediates RLP-induced, but not PDGF-induced, BVSMC migration. (A and B) BVSMCs were applied to the upper chamber of transwells whose lower chamber contained serum-free medium with or without (a), RLPs (25 μg/ml; b), n-VLDL (25 μg/ml; c), or PDGF-BB (3 ng/ml; d). Representative photomicrographs (A) and migrated cell numbers (B) from three independent experiments are shown (A). (C) After transfection with or without 100 nM of LOX-1 siRNA #1, LOX-1 siRNA #2, or control siRNA, BVSMCs were subjected to the transwell cell migration assay with RLPs (25 μg/ml) or PDGF-BB (3 ng/ml) for 8 h. (#) $p<0.0001$ vs. control, (##) $p<0.005$ vs. RLPs, (*) $p<0.05$ vs. RLPs without siRNAs, (†) $p<0.05$ vs. RLPs with control siRNA.

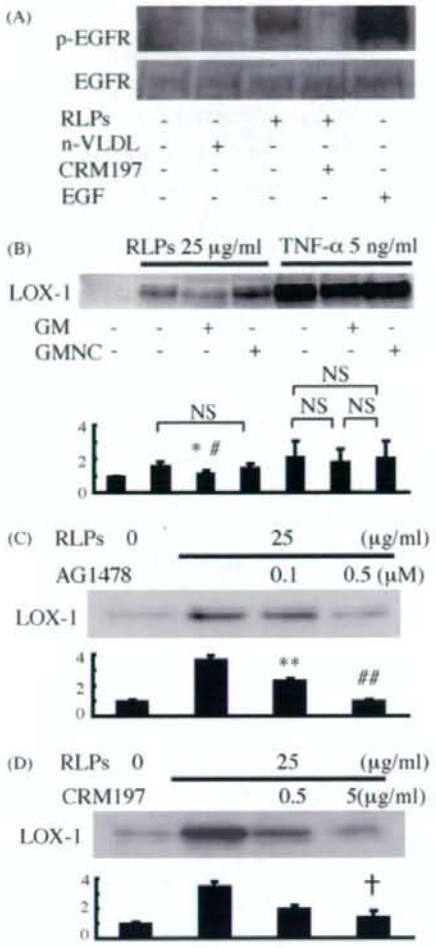

Fig. 4. Phosphorylation of EGFR induced by RLPs, and involvement of metalloproteinase activation, HB-EGF shedding and EGFR transactivation in RLP-induced LOX-1 expression. (A) BVSMCs were incubated with 25 μg/ml RLPs with or without 1 h-pretreatment with CRM197 (5 μg/ml), 25 μg/ml of n-VLDL, or 10 ng/ml of EGF for 5 min. Then, total cell lysates were subjected to immunoblotting for phosphorylated or total EGFR. (B–D) After pretreated with 50 μM of GM or GMNC for 12 h (B), or with the indicated concentrations of AG1478 (C) or CRM197 (D) for 1 h, BVSMCs were incubated with RLPs or TNF-α for 16 h. Total cell lysates were subjected to immunoblot analyses for LOX-1. (*) $p<0.05$ vs. RLPs without inhibitors, (#) $p<0.05$ vs. RLPs with GMNC, (**) $p<0.01$ and (##) $p<0.001$ vs. RLPs without AG1478, (†) $p<0.05$ vs. RLPs without CRM197.

kinase (JNK) and Akt elicited by RLPs were measured by immunoblotting. RLPs induced significant phosphorylation of ERK, p38 MAPK and Akt (Fig. 5A), but not JNK (data not shown). Furthermore, CRM197 significantly suppressed RLP-induced phosphorylation of these signals (data not shown). Dependency of RLP-induced LOX-1 expression upon ERK, p38 MAPK and PI3K was examined by specific inhibitors. As shown in Fig. 5B, PD98059, SB203580 and wortmannin, an inhibitor of MEK1, p38 MAPK and phosphoinositide 3-kinase (PI3K), respectively, significantly suppressed RLP-induced LOX-1 expression in BVSMC. These results indicate RLP-induced LOX-1 expression depends upon MEK1-ERK, p38 MAPK and PI3K-Akt cascades located downstream to the EGFR transactivation, respectively.

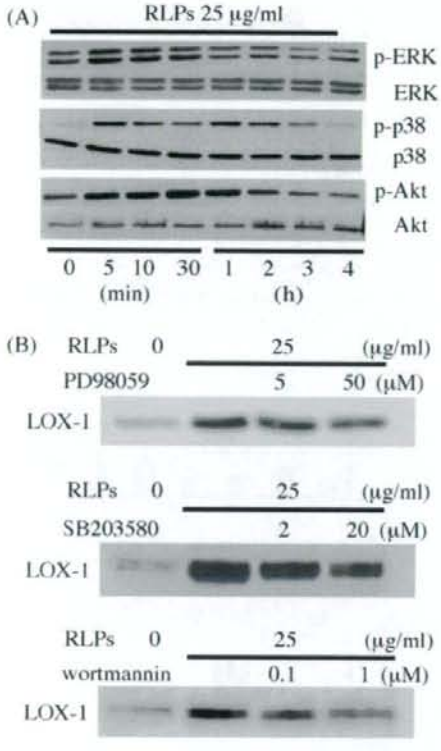

Fig. 5. Involvement of ERK, p38 MAPK and Akt phosphorylation in RLP-induced LOX-1 expression in BVSMCs. (A) After BVSMCs were incubated with 25 μg/ml of RLPs for the indicated periods, total cell lysates were subjected to immunoblot analyses for phosphorylated or total ERK, p38 MAPK and Akt. (B) After pretreated with the indicated concentrations of PD98059, SB203580 or wortmannin for 1 h, BVSMCs were incubated with RLPs (25 μg/ml) for 16 h and then subjected to immunoblotting for LOX-1.

3.7. Shedding of HB-EGF, EGFR transactivation and phosphorylation of ERK, p38 MAPK and Akt are involved in RLP-induced cell migration of BVSMCs

Pretreatment with GM, AG1478 and CRM197, but not GMNC, significantly suppressed RLP-induced VSMC migration (Fig. 6A and B). Furthermore, PD98059, SB203580 and wortmannin significantly suppressed migration of BVSMCs induced by RLPs (Fig. 6C). These results indicate RLP-induced BVSMC migration depends upon HB-EGF shedding, EGFR transactivation, and subsequent activation of MEK1-ERK, p38 MAPK and PI3K-Akt.

4. Discussion

In this study, we have provided the direct evidences that LOX-1 serves as a receptor for RLPs in VSMCs by use of two cell lines which stably express human or bovine LOX-1 and siRNA directed to LOX-1. In addition, we have shown

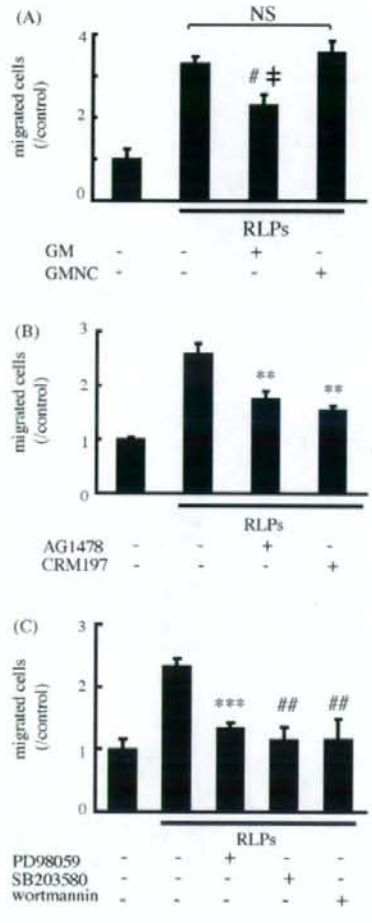

Fig. 6. Involvement of metalloproteinase activation, HB-EGF shedding, EGFR transactivation, and activation of ERK, p38 MAPK and PI3K in RLP-induced migration of BVSMCs. (A–C) After pretreatment with 50 μM of GM or GMNC for 12 h (A), AG1478 (0.5 μM) or CRM197 (5 μg/ml) for 1 h (B), or with PD98059 (50 μM), SB203580 (20 μM), or wortmannin (1 μM) for 1 h (C), BVSMCs were subjected to cell migration assay with RLPs (25 μg/ml) for 8 h. (#) $p < 0.005$ vs. RLPs without inhibitors, (‡) $p < 0.005$ vs. GMNC, (**) $p < 0.0001$, (***) $p < 0.001$, (##) $p < 0.005$ vs. RLPs without inhibitors.

that RLPs induce cell migration and LOX-1 expression by RLP-LOX-1 interactions, thus making a positive-feed back loop to further enhance the RLP-induced vascular dysfunction, as we already showed in oxidized LDL-induced vascular dysfunction [19].

In accordance with a previous report [9], we have demonstrated that RLP-induced LOX-1 expression and cell migration depend upon HB-EGF shedding and subsequent EGFR transactivation. Furthermore, we have shown the involvement of ERK, p38 MAPK and Akt as signal transducrion cascades located downstream to the EGFR transactivation. Furthermore, JNK was not activated by RLPs or not involved in RLP-induced LOX-1 expression or cell

migration (data not shown), indicating the specificity of the RLP-induced signals.

Competition studies in cells stably expressing LOX-1 indicated binding site(s) on the LOX-1 molecule for RLPs and oxidized LDL appear to be identical or overlapped, suggesting the C-terminal cysteine-rich C-type lectin-like domain may also be the responsible binding site(s) for RLPs [29], although the direct evidence should be provided in the future. Furthermore, previous studies have indicated that ADAMs are proteases responsible for HB-EGF shedding [30]; therefore, ADAMs may be involved in RLP-induced HB-EGF shedding. However, it remains to be fully elucidated which molecular mechanisms are involved after RLP-LOX-1 interactions to activate ADAMs which shed HB-EGF.

In summary, RLP-induced LOX-1 expression and VSMC migration appear to be important in atherogenesis elicited by postprandial hyperlipidemia, diabetes mellitus and metabolic syndrome. The present study has suggested the importance of LOX-1 in RLP-induced atherogenesis, as well as that induced by oxidized LDL. Further studies in suitable animal models, as well as clinical studies, would further elucidate the roles of LOX-1 in this process.

Acknowledgments

This work has been supported by Grants-in-Aid for Scientific Research (16590880, 18590985) from the Japanese Ministry of Education, Science, Sports, and Culture, and a research grant from Yokoyama Foundation for Clinical Pharmacology. We thank Kyoto Red Cross Blood Center for gift of unused human plasma.

Appendix A. Supplementary data

Supplementary data associated with this article can be found, in the online version, at doi:10.1016/j.atherosclerosis.2007.12.017.

References

[1] Kannel WB, McGee DL. Diabetes and cardiovascular disease, the Framingham study. JAMA 1979;41:2035–8.
[2] Alexander CM, Landsman PB, Teutsch SM, Haffner SM. NECP-defined metabolic syndrome, diabetes, and prevalence of coronary heart disease among NHANES III participants age 50 year and older. Diabetes 2003;52:1210–4.
[3] Nakajima K, Saito T, Tamura A, et al. Cholesterol in remnant-like lipoproteins in human serum using monoclonal anti apo B-100 and anti apo A-1 immunoaffinity mixed gels. Clin Chim Acta 1993;223:53–71.
[4] Nakamura T, Kugiyama K. Triglycerides and remnant particles as risk factors for coronary artery disease. Curr Atheroscler Rep 2006;8:107–10.
[5] Fukushima H, Sugiyama S, Honda O, et al. Prognostic value of remnant-like lipoprotein particle levels in patients with coronary artery disease and type II diabetes mellitus. J Am Coll Cardiol 2004;43:2219–24.
[6] Masuoka H, Kamei S. Predictive value of remnant-like particle cholesterol as an indicator of coronary artery stenosis in patients with normal serum triglyceride levels. Intern Med 2000;39:540–6.
[7] Higashi K, Ito T, Nakajima K, et al. Remnant-like particles cholesterol is higher in diabetic patients with coronary artery disease. Metabolism 2001;50:1462–5.
[8] Kawakami A, Tanaka A, Nakajima K, Shimokado K, Yoshida M. Atorvastatin attenuates remnant lipoprotein-induced monocyte adhesion to vascular endothelium under flow conditions. Circ Res 2002;91:263–71.
[9] Kawakami A, Tanaka A, Chiba T, et al. Remnant lipoprotein-induced smooth muscle cell proliferation involves epidermal growth factor receptor transactivation. Circulation 2003;108:2679–88.
[10] Kawakami A, Tani M, Chiba T, et al. Pitavastatin inhibits remnant lipoprotein-induced macrophage foam cell formation through ApoB48 receptor-dependent mechanism. Arterioscler Thromb Vasc Biol 2005;25:424–9.
[11] Tomono S, Kawazu S, Kato N, et al. Uptake of remnant like particles (RLP) in diabetic patients from mouse peritoneal macrophages. J Atheroscler Thromb 1994;1:98–102.
[12] Ross R. Atherosclerosis—an inflammatory disease. N Engl J Med 1999;340:115–26.
[13] Hussain MM, Maxfield FR, Mas-Oliva J, et al. Clearance of chylomicron remnants by the low density lipoprotein receptor-related protein/alpha 2-macroglobulin receptor. J Biol Chem 1991;266:13936–40.
[14] Gianturco SH, Ramprasad MP, Song R, et al. Apolipoprotein B-48 or its apolipoprotein B-100 equivalent mediates the binding of triglyceride-rich lipoproteins to their unique human monocyte-macrophage receptor. Arterioscler Thromb Vasc Biol 1998;18:968–76.
[15] Takahashi S, Sakai J, Fujino T, et al. The very low-density lipoprotein (VLDL) receptor: characterization and functions as a peripheral lipoprotein receptor. J Atheroscler Thromb 2004;11:200–8.
[16] Sawamura T, Kume N, Aoyama T, et al. An endothelial receptor for oxidized low-density lipoprotein. Nature 1997;386:73–7.
[17] Moriwaki H, Kume N, Sawamura T, et al. Ligand specificity of LOX-1, a novel endothelial receptor for oxidized low density lipoprotein. Arterioscler Thromb Vasc Biol 1998;18:1541–7.
[18] Moriwaki H, Kume N, Kataoka H, et al. Expression of lectin-like oxidized low density lipoprotein receptor-1 in human and murine macrophages: upregulated expression by TNF-α. FEBS Lett 1998;440:29–32.
[19] Kataoka H, Kume N, Miyamoto S, et al. Oxidized LDL modulates Bax/Bcl-2 through the lectinlike Ox-LDL receptor-1 in vascular smooth muscle cells. Arterioscler Thromb Vasc Biol 2001;21:955–60.
[20] Kume N, Kita T. Apoptosis of vascular cells by oxidized LDL: involvement of caspases and LOX-1 and its implication in atherosclerotic plaque rupture. Circ Res 2004;94:269–70.
[21] Kume N, Murase T, Moriwaki H, et al. Inducible expression of lectin-like oxidized LDL receptor-1 in vascular endothelial cells. Circ Res 1998;83:322–37.
[22] Mukai E, Kume N, Hayashida K, et al. Heparin-binding EGF-like growth factor induces expression of lectin-like oxidized LDL receptor-1 in vascular smooth muscle cells. Atherosclerosis 2004;176:289–96.
[23] Aoyama T, Fujiwara H, Masaki T, Sawamura T. Induction of lectin-like oxidized LDL receptor by oxidized LDL and lysophosphatidylcholine in cultured endothelial cells. J Mol Cell Cardiol 1999;31:2101–14.
[24] Kataoka H, Kume N, Miyamoto S, et al. Expression of lectinlike oxidized low-density lipoprotein receptor-1 in human atherosclerotic lesions. Circulation 1999;99:3110–7.
[25] Shin HK, Kim YK, Kim KY, Lee JH, Hong KW. Remnant lipoprotein particles induce apoptosis in endothelial cells by NAD(P)H oxidase-mediated production of superoxide and cytokines via lectin-like oxidized low-density lipoprotein receptor-1 activation: prevention by cilostazol. Circulation 2004;109:1022–8.

[26] Park SY, Lee JH, Kim YK, et al. Cilostazol prevents remnant lipoprotein particle-induced monocyte adhesion to endothelial cells by suppression of adhesion molecules and monocyte chemoattractant protein-1 expression via lectin-like receptor for oxidized low-density lipoprotein receptor activation. J Pharmacol Exp Ther 2005;312:1241–8.
[27] Jawien A, Bowen-Pope DF, Lindner V, Schwartz SM, Clowes AW. Platelet-derived growth factor promotes smooth muscle migration and intimal thickening in a rat model of balloon angioplasty. J Clin Invest 1992;89:507–11.
[28] Redmond EM, Cahill PA, Hirsch M, et al. Effect of pulse pressure on vascular smooth muscle cell migration: the role of urokinase and matrix metalloproteinase. Thromb Haemost 1999;81:293–300.
[29] Chen M, Narumiya S, Masaki T, Sawamura T. Conserved C-terminal residues within the lectin-like domain of LOX-1 are essential for oxidized low-density-lipoprotein binding. Biochem J 2001;355:289–96.
[30] Higashiyama S, Nanba D. ADAM-mediated ectodomain shedding of HB-EGF in receptor cross-talk. Biochim Biophys Acta 2005; 1751:110–7.